Redistribution of TPA Fluxes in the Presence of PAI-1 Regulates Spatial Thrombolysis

Shibeko, A.M.; Chopard, B.; Hoekstra, A.G.; Panteleev, M.A.

DOI
10.1016/j.bpj.2020.06.020

Publication date
2020

Document Version
Final published version

Published in
Biophysical Journal

Biophysical Journal
Article

Biophysical Society

Redistribution of TPA Fluxes in the Presence of PAI-1 Regulates Spatial Thrombolysis

Alexey M. Shibeko,[1,2] Bastien Chopard,[3] Alfons G. Hoekstra,[4] and Mikhail A. Panteleev[1,2,5,6,*]

[1]Center for Theoretical Problems of Physico-Chemical Pharmacology, Russian Academy of Sciences, Moscow, Russia; [2]Dmitry Rogachev National Medical Research Centre of Pediatric Hematology, Oncology and Immunology, Moscow, Russia; [3]Computer Science Department, University of Geneva, Carouge, Switzerland; [4]Computational Science Lab, Institute for Informatics, Faculty of Science, University of Amsterdam, Amsterdam, the Netherlands; [5]Faculty of Physics, Lomonosov Moscow State University, Moscow, Russia; and [6]Faculty of Biological and Medical Physics, Moscow Institute of Physics and Technology, Dolgoprudnyi, Russia

ABSTRACT The fibrin clot is gelatinous matter formed upon injury to stop blood loss and is later destroyed by fibrinolysis, an enzymatic cascade with feedback. Pharmacological fibrinolysis stimulation is also used to destroy pathological, life-threatening clots and thrombi (thrombolysis). The regulation of the nonlinear spatially nonuniform fibrinolytic process in thrombolysis is not currently well understood. We developed a reaction-diffusion-advection model of thrombolysis by tissue plasminogen activator (TPA) in an occluded vessel with a pressure gradient. Sensitivity-analysis-based model reduction was used to reveal the critical processes controlling different steps of thrombolysis. The propagation of thrombolysis in the system without flow was predominantly controlled by TPA diffusion, whereas transport of other active components was rendered nonessential either by their high fibrin-binding parameters and short lifetimes or their initial uniform distribution. The concentration of the main TPA inhibitor plasminogen activator inhibitor 1 (PAI-1) controlled both the extent of lysis propagation and the shape of fibrin spatial distribution during lysis. Interestingly, PAI-1 remained important even when its concentration was an order of magnitude below that of TPA because of its role at the edge of the diffusing TPA front. The system was robust to reaction rate constant perturbations. Using these data, a reduced model of thrombolysis was proposed. In the presence of flow, convection of TPA was the critical controlling process; although the role of PAI-1 concentration was much less in the presence of flow, its influence became greater in the presence of collateral bypassing vessels, which sufficiently reduced TPA flux through the thrombus. Flow bypass through the collateral vessel caused a decrease in TPA flux in the clotted vessel, which increased the PAI-1/TPA ratio, thus making PAI-1-induced inhibition relevant for the regulation of spatial lysis up to its arrest.

SIGNIFICANCE The successful fibrinolysis of life-threatening thrombi determines recovery after stroke or infarction. In this work, we employ an in silico model of spatial fibrin clot lysis to determine the mechanisms of its regulation and show that clot lysis is controlled by the transport and inhibition of the thrombolytic agent. Vascular surroundings, such as bypassing vessels, may downregulate thrombolytic flow through the clot, whereas elevated concentrations of thrombolytic inhibitors may diminish thrombolytic penetration inside the clot. These effects may cause complete arrest of clot lysis.

INTRODUCTION

The critical element in the physiological response of blood to vascular injury is a consecutive fluid-gel-fluid transition, which involves first the formation of branched polymers of fibrin molecules (to create a hemostatic plug barrier once the blood-body boundary has been breached) and then their degradation (once the tissue has been repaired) to restore the initial state of the vascular system. Fibrin polymerization is controlled by blood coagulation, a complex cascade of proteolytic reactions regulated by several positive and negative feedback loops, which is triggered by extravascular protein tissue factor (1,2). Fibrin clots can also be formed inside vessels as a result of pathological processes and thus lead to thrombosis, which eventually may result in myocardial infarction or ischemic stroke. The fibrinolytic system is a network of biochemical reactions in blood plasma that functions to disintegrate a fibrin clot when it is unwanted or when it is no longer needed (3). The lysis process is initiated by two enzymes, tissue plasminogen activator (TPA) released by the vascular wall and urokinase plasminogen activator present in a precursor form in blood (4). The

Submitted January 30, 2020, and accepted for publication June 16, 2020.

*Correspondence: mapanteleev@yandex.ru

Editor: Mark Alber.

https://doi.org/10.1016/j.bpj.2020.06.020

backbone of this network is also a cascade with positive feedback loops that ultimately converts the inactive enzyme precursor glu-plasminogen (PgG) into serine protease plasmin (Pn) capable of cleaving fibrin molecules (5). Pn itself can partially activate PgG to lys-plasminogen (PgL), which is more efficiently activated to Pn by TPA (6). A critical trigger and cofactor of lysis is fibrin itself, which binds Pn and protects it from inactivation (7) by α-2-antiplasmin (α_2AP) and α-2-macroglobulin (α_2M). It also binds both plasminogen (PgG_B) and TPA (TPA_B), which accelerates the activation of plasminogen by TPA by three orders of magnitude (8) and protects TPA from inactivation by plasminogen activator inhibitor 1 (PAI-1) (9). The fibrinolysis system is also involved in immunity, tissue remodeling, and other roles beyond hemostasis (10,11).

Because of the low rate of TPA secretion (12,13), the physiological timescale of fibrinolysis is tens of hours. One of the main therapeutic approaches to treating dangerous clots, thrombi, which block blood flow in crucial vessels and cause ischemic stroke or myocardial infarction, is the injection of supraphysiological amounts of fibrinolysis activators, mostly TPA and its variants (14,15). However, for ischemic strokes, this treatment should be performed within 3 h after vessel occlusion (16) and has a success rate of less than 50% (17). It is not clear why some clots are resistant to lysis. One of the main problems in the development and application of new treatment strategies is insufficient understanding of the regulation of underlying processes. Fibrinolysis is a complex, spatially nonuniform phenomenon, and both transport processes and nonlinear reaction kinetics with feedback loops could fundamentally complicate the system response, as suggested by previous mathematical models and experimental studies of its regulation.

In a previous work (18), in vitro and in silico setups were combined to elucidate the mechanisms of spatial clot formation in the presence of therapeutic concentrations of TPA. The simultaneous propagation of clot growth and lysis fronts was observed. The model in this study was derived from the previous model (18) with modifications: the thrombin generation and fibrin formation modules were excluded, and a flow of liquid described by Darcy's law was implemented. A multiscale model starting from a single-fiber cross section and proceeding to a three-dimensional (3D) fibrin clot (19) was used to demonstrate that the rate of spatial lysis front propagation depended on the local TPA concentration, which was determined by plasmin-induced fibrin degradation (20). This model detailed the interaction of fibrin with TPA, plasminogen, and Pn, but lysis inhibition by α2AP, α2M, and PAI-1, as well as the impact of flow, were beyond the scope of the study. A one-dimensional (1D) model of fibrin clot lysis describing the diffusion and convection of reagents through porous medium showed that pressure-driven permeation was the primary determinant of the overall rate of clot lysis (21). Different regimes of TPA and urokinase plasminogen activator administration were applied for arterial and venous thrombi. The model predicted the measured lysis front movement and the eventual depletion of α2AP and α2M in an advancing lysis zone (22). A 3D thrombolysis model in a patient-specific geometry evaluating the effects of TPA dose on the efficacy of thrombolytic therapy and the risk of intracerebral hemorrhage was developed in (23). Applying this model to a fibrin clot with two different fibrin fibril radii, authors found that clot lysis was driven by TPA penetration in the clot; it was facilitated either by increased TPA dose or by higher permeability of coarse fibrin clot. The model proposed in this study included detailed chemical reactions of TPA, PAI-1, fibrin, plasmin(ogen), and α2AP interactions in the presence of diffusion and advection in 1D or 3D geometry.

The objective of the current study was to employ biophysical approaches to identify the crucial processes that regulate spatial fibrinolysis and to understand the impact of the physical properties of the clot and of the surrounding vessels on the outcome of thrombolytic therapy. To investigate the basic mechanisms of this regulation, we simulated therapeutic fibrin clot dissolution using a mathematical model in which spatially nonuniform lysis of a preformed clot in a vessel was induced by the TPA able to penetrate the clot by means of diffusion and advection.

METHODS

Mathematical simulation

General description

The following models employed in this study shared common biochemistry (except for reductions when indicated) but differed in their spatial arrangement, simulation of flow, and transport conditions:

1) one-dimensional models of thrombolysis,
A. full lysis model with/without flow,
B. reduced lysis model with/without flow,
C. reduced lysis model with flow and pharmacokinetic conditions for TPA,
2) and three-dimensional model of thrombolysis.

A reduced lysis model with flow in the presence/absence of collateral flow. For these simulations, we developed a set of modules that described certain processes of spatial fibrinolysis and employed them in different combinations. The spatial setup for the one-dimensional model is described in Fig. 1 *A*. Initially, the left half of the domain is occupied by the fibrin clot, whereas the blood with TPA is in the right half of the domain.

Biochemical module: detailed version

This module describes the biochemical reactions of fibrin clot dissolution. The chemical design of the model, as shown in Fig. 1 *B*, is based on our previous model (18), with modifications. Briefly, TPA is able to diffuse and bind to fibrin and is inhibited by PAI-1. TPA is also able to convert PgG to Pn. Pn can also bind to fibrin, be inhibited by α2M and α2AP, and cleave fibrin. Fibrin itself can augment the lysis process, as it not only protects Pn from inactivation (7) but also accelerates the activation of PgG by TPA by an order of 500 (8), as shown in Fig. 1 *B* with a wider arrow. All species except fibrin and fibrin-bound molecules are allowed to diffuse. The set of equations describing this module are Eqs. S1–S12.

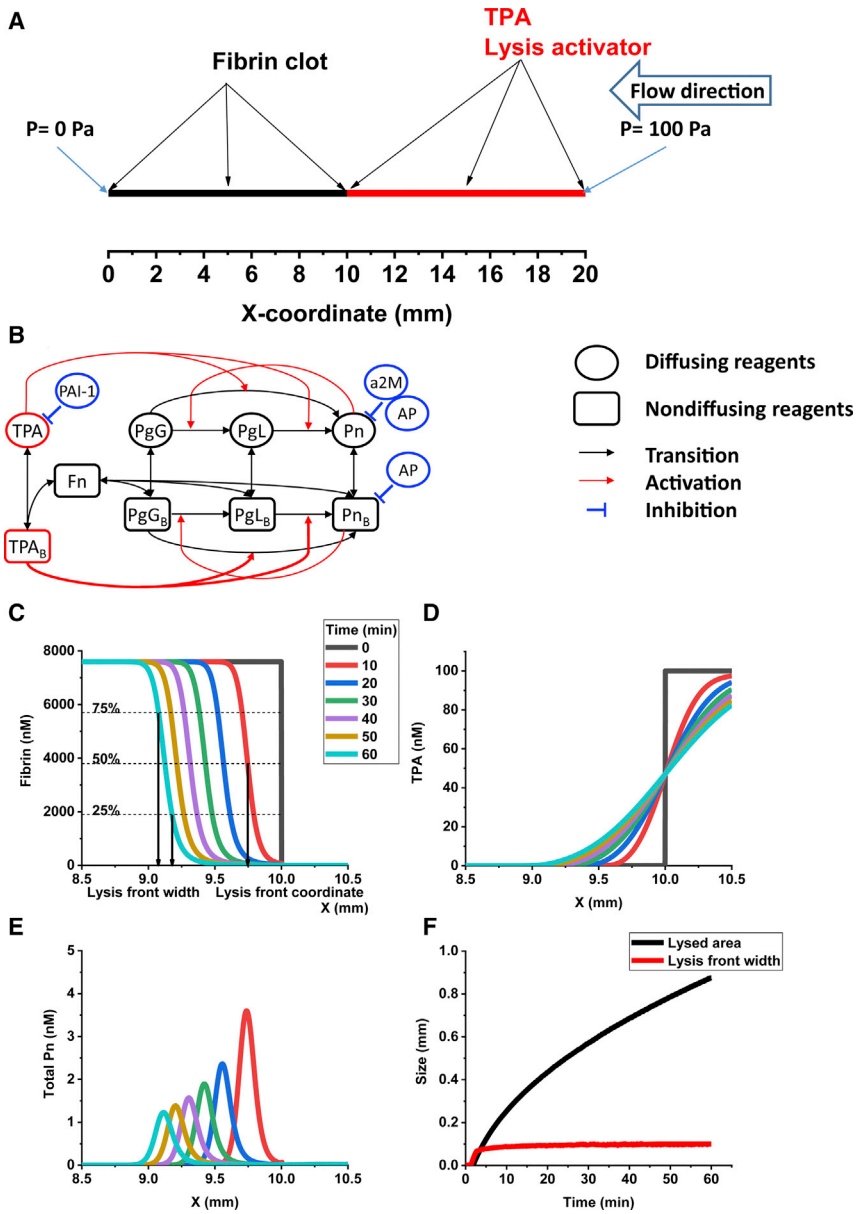

FIGURE 1 Lysis of a fibrin clot in the 1D model. (*A*) Simulation setup. A fibrin clot is located from x = 0 to x = 10, whereas a lysis activator (TPA) is located in the area from x = 10 to x = 20. Flow through the clot (in simulations with flow) is described by Darcy's law and appears to occur because of a pressure difference. At x = 20 mm, $p = 100$ Pa, and at x = 0 mm, $p = 0$ Pa. (*B*) Scheme of reactions of the detailed model of spatial fibrin clot lysis. Diffusing and flow-transported reagents are shown as round shapes; nondiffusing reagents not transported via flow are shown as rectangular shapes. The transition from the inactive to activated form, a reversible complex formation, is shown with black arrows; the activation of a reaction is shown with red arrows, and activating reagents are shown in red shapes; and the inhibition of a reaction is shown with blue arrows and inhibitors in blue shapes. A detailed description of the model can be found in Figs. S1–S12. (*C*) Fibrin concentration profiles shown every 10 min after simulation onset. Lysis was initiated with 100 nM TPA in the absence of flow. The lysis front is located at the position where the fibrin concentration is reduced to half of the initial value. The lysis area size (LAS) can be calculated by subtracting the lysis front coordinate from 10 (its initial position). Lysis front width (LFW) was defined as the difference in coordinates in which fibrin concentration was within the range of 25 and 75% of initial. (*D*) TPA concentration profiles shown every 10 min after simulation onset. (*E*) Total Pn (free and bound with fibrin) concentration profiles shown every 10 min after simulation onset. (*F*) Time dependence of LAS (*black*) and LFW (*red*). To see this figure in color, go online.

Biochemical module: reduced version

After the process described in Necessity Analysis and Model Reduction and Analysis of the Reduced Model of the Results, we arrived at the reduced version of the fibrin clot lysis model, shown in Fig. 2 *A*. This module consisted of three ordinary differential equations, two partial differential equations (PDEs) and a constraint equation. A set of equations describing this module is listed in Necessity Analysis and Model Reduction (Eqs. 7, 8, 9, 10, 11, and 12).

Flow module

Blood flow was modeled as a process of liquid permeation through a porous medium (the clot), described by Darcy's law. A detailed description can be found in the Supporting Materials and Methods. On the right boundary, Dirichlet conditions for the transportable reagents TPA, PgG, PAI-1, and α_2M and α_2AP were set, and their boundary concentrations were equal to the initial condition because of constant refreshment of all fibrinolysis factors and continuous infusion of TPA. The clot permeability was in the range of 10^{-14}–10^{-12} m^2 (24–26), and the initial clot porosity was 0.99 (21). In our simulations, we used mostly one value for hydrostatic pressure difference and several values for clot permeability, but our calculations showed that an increase in hydrostatic pressure difference was identical to an increase in clot permeability (Fig. S6), which expanded the range of applicability of our results.

Pharmacokinetics module

Thrombolytic therapy during myocardial infarction includes a 15-mg bolus of TPA, followed by a 50-mg infusion within 30 min and a 35-mg infusion within 60 min (27). With a half-life of TPA $t_{1/2} = 5$ min (28) and a measured activity after a 15-mg bolus (30 nM) (27), we calculated boundary conditions for TPA in our simulation of thrombolytic therapy as follows: initial TPA concentration 30 nM, right boundary Dirichlet condition TPA = 30 nM (time <30 min), and right boundary Dirichlet condition TPA = 10 nM (time >30 min), which corresponds to the TPA infusion profile

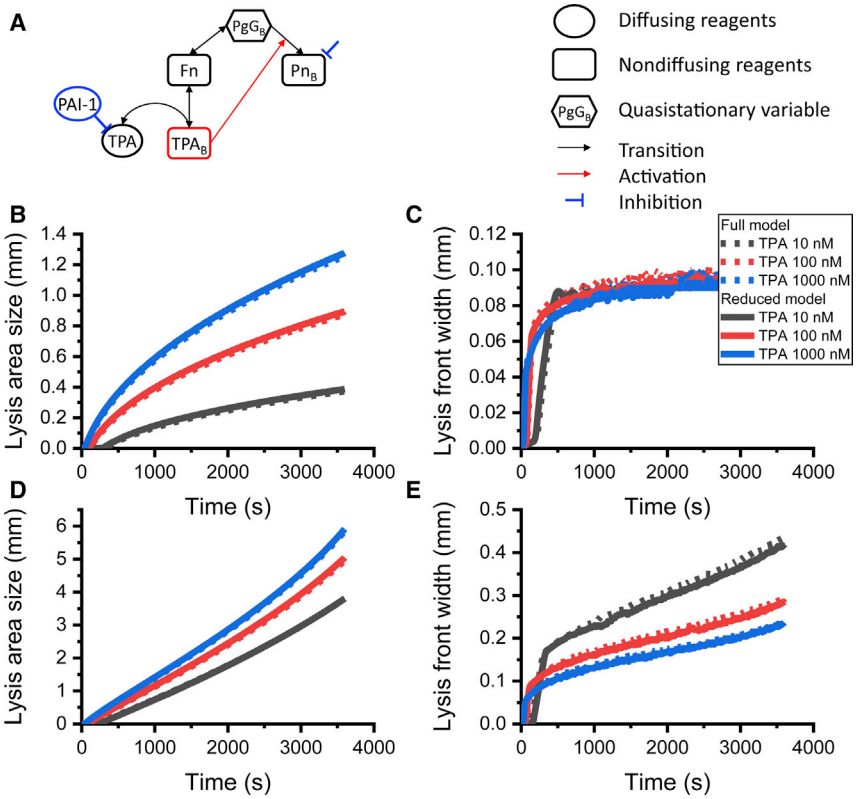

FIGURE 2 Comparison of lysis in detailed and reduced models. (*A*) Scheme of reactions of the reduced model of spatial fibrin clot lysis. Diffusion-driven lysis without flow, time course of LAS (*B*), and LFW (*C*). Advection-driven lysis in the presence of flow, time course of LAS (*D*), and LFW (*E*). The hydrostatic pressure difference was 100 Pa. The initial fibrin clot porosity was 0.99, and the permeability was 10^{-13} m^2. Detailed model (*dashed lines*) and reduced model (*solid lines*). The initial and inflowing TPA concentrations were 10 nM (*black lines*), 100 nM (*red lines*), or 1000 nM (*blue lines*). Simulations were performed in the 1D model. To see this figure in color, go online.

(27). TPA and PAI-1 were under open boundary conditions at x = 0; these conditions were equivalent to the outflow condition.

3D lysis

A full three-dimensional model was used to estimate the impact of collateral flow on TPA-induced fibrin clot lysis. The corresponding modifications were made in the equations of the reduced model of clot lysis (Eqs. 7, 8, 9, 10, 11, and 12); this model can be found in the Supporting Materials and Methods, Eqs. S44–S49.

We used three types of simulation areas (Fig. 5, *A–C*) consisting of one or two cylindrical vessels 1000 μm long and 200 μm in diameter with a 200-μm-long inlet vessel and junction on the right and a symmetric outlet on the left (a separate outlet for case C). These areas represented arteriole junctions (29,30).

Laminar flow of Newtonian blood was directed along the *Xx* axis to the origin, and it could enter either the upper vessel with a 1-mm long fibrin clot or the unclotted lower vessel. The pressure difference between the inlet (the right opening at x = 1350 μm) and the outlet (left opening at x = 0) was 10 Pa. There were no slip conditions for the flow (u = 0) on all boundaries of the simulation area except for the inlet and outlet. The initial TPA concentration in the simulation area was 0 nM. Fibrin (7600 nM) was localized in the upper vessel in a cylindrical area 1000 μm long and with a 200 μm diameter. The initial concentration of PAI-1 was 2 nM. The right boundary Dirichlet condition at X = 1350 μm was 30 nM for TPA and 2 nM for PAI-1. Open boundary conditions for TPA and PAI-1 equivalent to the outflow condition were imposed at X = −200 μm.

Simulation output parameters

During the simulations, the time-dependent spatial distribution of the concentration of each reagent concentration was recorded (e.g., distribution of TPA, Pn, and fibrin). To evaluate the efficiency of lysis, the spatiotemporal distribution of fibrin was transformed into kinetics of the propagation of the lysis front using the following rules. We assume that lysis occurs as soon as the local fibrin concentration is lower than 50% of the initial concentration, i.e., when 50% fibrin is dissolved (31). The position of the zone where fibrin concentration is half the initial value is the coordinate of the lysis front. Plotting the movement of the lysis front coordinate over time (considering its initial position at x = 10 mm as 0 and its movement inside the clot toward x = 0 as an increase in coordinate), the LAS as a function of time was obtained (Fig. 1 *F*). LFW represents the difference in coordinates where fibrin concentration was within the range of 25–75% of the initial value. This interval, in which fibrin concentration is below the initial one but higher than zero, is a zone of a "weak" clot, with a smaller amount of fibrin within it. This "weak" clot will, of course, have different mechanical properties from the initial clot: it becomes less resistant to shear stress, and a narrow lysis front, i.e., a narrow area of the "weak" clot, is considered preferable for lysis. To estimate the sensitivity coefficients C^S and C^W and necessity coefficients R^S and R^W as described in the Results, we used the endpoint value (at time 3600 s) for LAS and the average (within time interval 3000–3600 s) value for LFW. The lysis onset, the time when the lysis front started to move, was measured. In 3D lysis, we measured the recanalization time, the moment when the average flow velocity through the clotted vessel equilibrated with the flow velocity through the clot-free vessel.

Comsol parameters of simulation and numeric methods

Simulations were performed with Comsol 5.3 (Comsol, Burlington, MA).

In our 1D simulations, we used the absolute tolerance factor 4×10^{-6} (scaled) and the relative tolerance 0.01. The time stepping method was generalized α (which contains a parameter, called α in the literature, to control the degree of damping of high frequencies) with strict steps. Equations were solved using multifrontal massively parallel sparse direct solver (MUMPS). We used an area 20 mm long with an equidistant mesh of 2000 nodes.

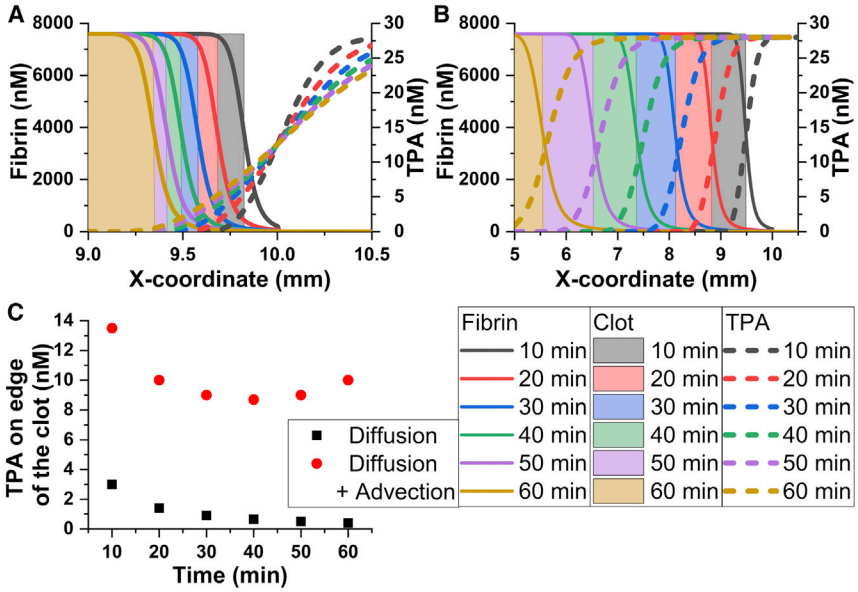

FIGURE 3 Dynamics of fibrin clot lysis in the absence of flow (*A*) or in the presence of flow (*B*). The fibrin distribution (*solid lines*) and TPA distribution (*dashed lines*) are shown for every 10 min of simulation. The filled area represents the current clot size (i.e., the area where the fibrin concentration is above 50% of the initial concentration). (*C*) TPA concentration on the edge of the solid clot in the absence of flow (*black*) and in the presence of flow (*red*). Its increase in the presence of flow after 40 min of simulation is caused by partial clot dissolution, which increased the overall clot permeability. Simulations were performed in the 1D model. The TPA concentration outside the clot was 30 nM. The hydrostatic pressure difference was 100 Pa, and the clot permeability was 10^{-13} m^2. To see this figure in color, go online.

In our 3D simulations, we used an absolute tolerance factor of 0.05 (scaled) and a relative tolerance of 0.005. The time stepping method was the backward differentiation formula with free steps. Free time stepping allows the solver to take larger or smaller time steps as required to satisfy the specified tolerances. Equations were solved using parallel direct sparse solver (PARDISO). Simulations were carried out in three different volumes, as shown in Fig. 5, *A–C*. The vessel diameter was 200 μm, and the length of the occlusive fibrin clot was 1 mm. We used a tetrahedral mesh with element sizes from 1.26×10^{-5} m up to 4.11×10^{-5} m in the unclotted area and from 6.32×10^{-6} m up to 2.12×10^{-5} m in the area with a fibrin clot.

RESULTS

A biophysical model of spatially nonuniform fibrin clot lysis by TPA

As a first step, we implemented a mathematical model capturing the essential aspects of clot lysis biophysics. The model considers a one-dimensional chamber composed of two compartments, clot and fluid blood (Fig. 1 *A*), which represented an occluded vessel. To the right compartment of the model, TPA was added at time 0 to mimic the start of thrombolytic therapy. The model comprises two equation modules, one describing the reactions and transport of species (as described in the scheme of Fig. 1 *B*) and the other describing the flow of blood through the porous medium of the clot. Detailed descriptions of the model can be found in the Methods. Model equations are Eqs. S1–S12.

Representative dynamics of clot lysis initiated by 100 nM TPA are shown in Fig. 1 *C*. Slow diffusional penetration of TPA into the clot leads to gradual clot dissolution (Fig. 1 *D*) by Pn, which is distributed as a propagating decaying peak (Fig. 1 *E*). This process can be characterized by the propagation curve of the lysis front moving at a slowly decelerated pace and by the front width time course, which had a characteristic scale of 0.1 mm throughout the lysis process (Fig. 1 *F*).

Sensitivity analysis

We next performed sensitivity analysis (as described in (32)) to find the regulating parameters of the system. Detailed analysis is presented in the Supporting Materials and Methods; briefly, we calculated LAS and LFW while increasing and decreasing each parameter's value from 1% up to 10%. Based on these values, we calculated C^S and C^W as follows:

$$C^S_{i\%} = \frac{LAS_{(100+i)\%} - LAS_{(100-i)\%}}{0.02 \times i \times LAS_{100\%}}, \quad (1)$$

$$C^W_{i\%} = \frac{LFW_{(100+i)\%} - LFW_{(100-i)\%}}{0.02 \times i \times LFW_{100\%}}. \quad (2)$$

The coefficient C^S showed the impact of the parameter on the lysis propagation (lysis velocity), and the coefficient C^W showed the impact of the parameter on the quality of clot dissolution. We performed this analysis in a spatially distributed system in the absence of flow using 100 nM TPA. The results are presented in Figs. S1–S5. There were almost no changes in sensitivity as the parameter variation increased from 3 to 10%; thus, we next chose a parameter variation of 5% for detailed analysis using TPA concentrations of 10, 100, and 1000 nM (Table S5 shows coefficients for the case without flow, and Table S6 shows coefficients for the case with flow). The hydrostatic pressure difference was 100 Pa. The initial fibrin clot porosity was 0.99, and the permeability was 10^{-13} m^2.

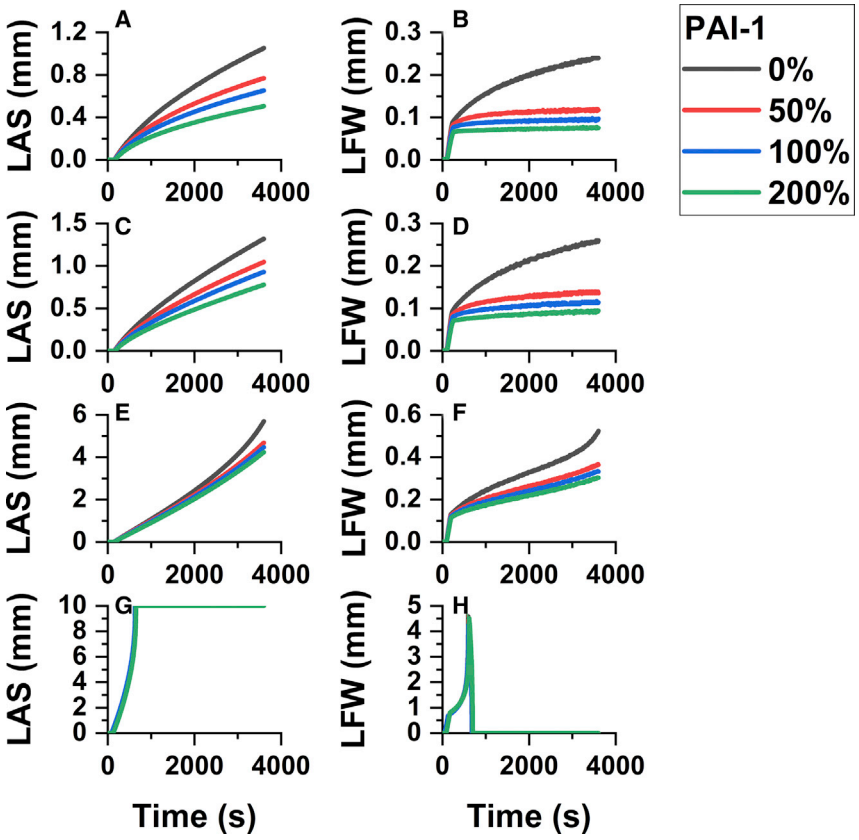

FIGURE 4 The effect of PAI-1 on spatial clot lysis depends on physical conditions. The LAS (*A*, *C*, *E*, and *G*) and LFW (*B*, *D*, *F*, and *H*) are shown. The PAI-1 concentration was 0 nM (*black lines*), 1 nM (50% of normal) (*red lines*), 2 nM (100% of normal) (*blue lines*), or 4 nM (200% of normal) (*cyan lines*). Simulations were carried out for no-flow conditions (*A* and *B*) and with flow under a hydrostatic pressure difference of 10 Pa (*C* and *D*), 100 Pa (*E* and *F*), or 1000 Pa (*G* and *H*). Simulations were performed in the 1D model. The initial fibrin clot porosity was 0.99. The clot permeability was 10^{-13} m^2. For these simulations, a reduced model of fibrin clot lysis coupled with the pharmacokinetics module for TPA was used. The initial TPA concentration was 30 nM, and the right boundary condition for TPA inflow was 30 nM (time <30 min) and 10 nM (time >30 min). To see this figure in color, go online.

Briefly, we found that lysis propagation was sensitive to variation in very few parameters (initial concentration of TPA and PAI-1, diffusion of TPA) (Table 1), which can be considered long-range regulatory parameters. The LFW was sensitive to a greater number of parameters (Table 2). Most of them had no impact on lysis propagation, and we can consider them local regulatory parameters, which regulate the length of a "weak" clot but not the overall lysis efficacy.

The initial concentration of fibrin had a negative impact on the LFW because an increased amount of fibrin bound more TPA, and its distribution inside the clot was narrower. The same effect was caused by the association rate of TPA with fibrin ($k_a^{TPA,\ Fn}$). Similarly, the catalytic rate of the activation of PgG bound with fibrin by TPA bound with fibrin ($k_{cat}^{PgG_B,\ TPA_B}$) had a negative impact on the LFW as more Pn was activated and clot dissolution occurred faster.

The initial α2AP concentration had a positive impact on LFW because it could inhibit Pn bound with fibrin, thus reducing the rate of fibrin degradation. The same effect was caused by the inhibition rate of Pn bound with fibrin ($k_i^{Pn_B,\ \alpha_2AP}$), and the opposite effect was caused by the rate of fibrin degradation ($k_{cat}^{Fn,\ \ Pn}$), which increased the LFW.

TPA concentration in the absence of flow had a significant positive impact on lysis propagation, but in the presence of flow, this impact was negligible. Interestingly, its impact on the LFW was absent without flow but appeared under flow conditions. The PAI-1 concentration had a significant negative impact on lysis propagation and a significant negative impact on LFW without flow, but in the presence of flow, only a moderate impact on LFW was revealed. This inhibitor demonstrated both local and global impacts on lysis for low TPA concentrations, switching only to local effects with increasing TPA concentration (because of an increase in initial TPA concentration or acceleration of TPA transportation by flow). The mechanisms of such behavior of PAI-1 will be discussed in Analysis of the Reduced Model. Finally, the diffusion of TPA had a critical effect on both lysis propagation and LFW, whereas other diffusion coefficients had negligible impacts. The diffusion of TPA is the only means for lysis propagation, which is why this parameter regulates all processes, including the local length of a "weak" clot and global lysis efficacy. Interestingly, in the presence of flow, the impact of TPA diffusion decreased but remained significant.

It is worth mentioning that all species except for Fn and α2M had a significant effect on the lysis propagation in the absence of flow and for low TPA concentration (10 nM), but this effect sufficiently decreased with TPA concentration increase, and it was absent in the presence of flow, even for low TPA concentration. We

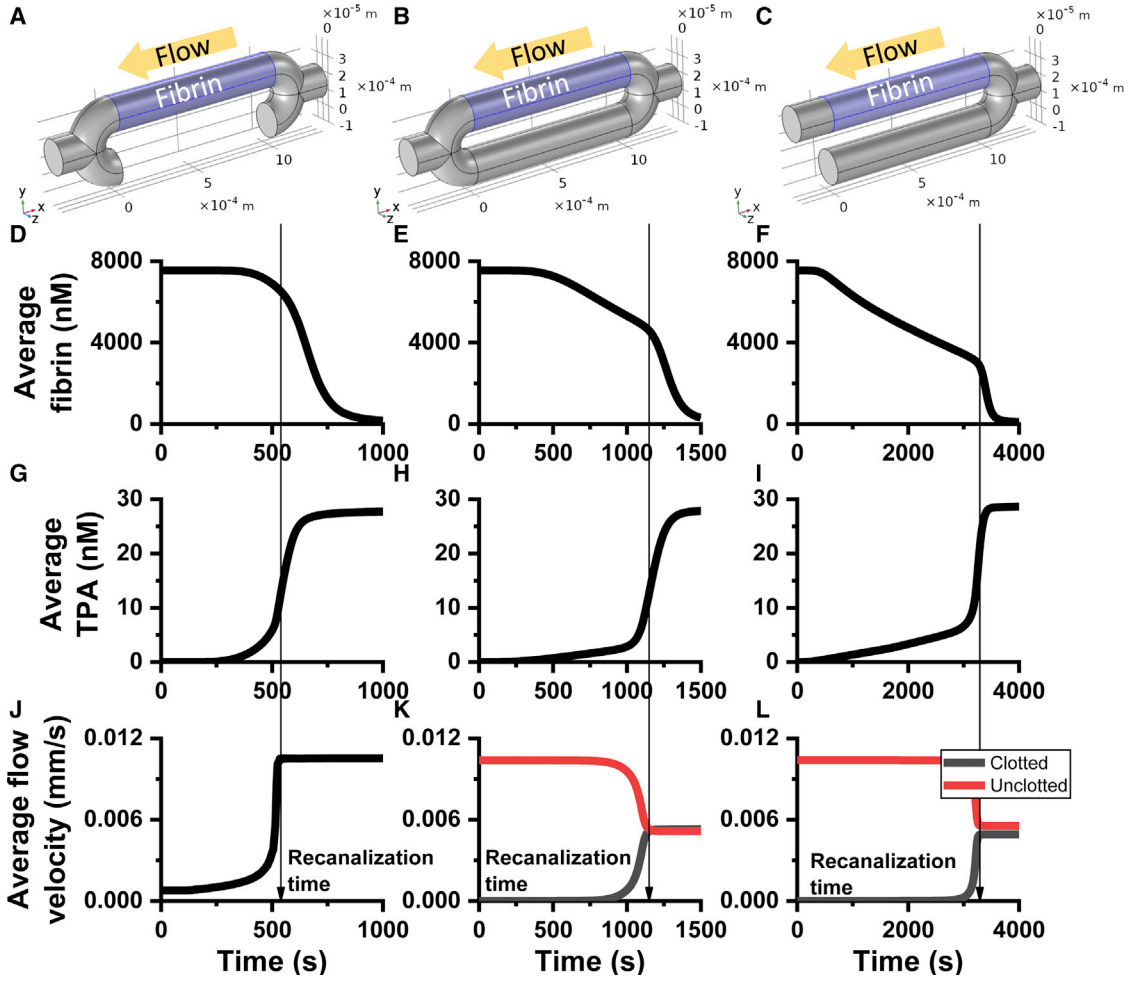

FIGURE 5 Spatial lysis in the chamber with a single channel (*A*), with collateral channels and a single exit (*B*) or in a chamber with collateral channels and separate exits (*C*). Time course of the average fibrin concentration in the occluded vessel is shown in (*D*)–(*F*); average free TPA concentration in the occluded vessel is shown in (*G*)–(*I*); average flow velocity in the occluded and bypassing vessels is shown in (*J*)–(*L*). Simulations were performed in the 3D model. The hydrostatic pressure difference was 10 Pa, the clot permeability was 10^{-13} m^2, and the initial clot porosity was 0.99. The chamber was constructed from tubes 200 μm in diameter, and the initial fibrin clot length was 1 mm. To see this figure in color, go online.

assume that when TPA transport is limited to the diffusion only, low amount of TPA on the edge of the clot initiates lysis slowly, and it can be easily facilitated or slowed down by small changes in initial concentrations of the species.

Necessity analysis and model reduction

As our analysis in Sensitivity Analysis demonstrated, only very few parameters of the model regulated the behavior of the lysis process. To simplify the model and to outline the most important reactions and reagents, we performed a necessity analysis (32) of this system in the absence of flow and under flow conditions by removing some reactions and components. The initial TPA concentration was 30 nM, and the hydrostatic pressure difference was 0 or 100 Pa. The initial fibrin clot porosity was 0.99, and the fibrin clot permeability was 10^{-13} m^2. As a system output, we used the LAS and LFW. Necessity coefficients R^S and R^W were used to estimate the impact of the flux of reagent j (chemical reaction, diffusion, or advection that changes the concentration of reagent j) or the reagent itself.

$$\frac{\partial [TPA]}{\partial t} = D_{TPA} \times \frac{\partial^2 [TPA]}{\partial x^2} - u \times \frac{\partial [TPA]}{\partial x}$$

$$-k_i^{TPA,\ PAI1} \times [TPA] \times [PAI-1] - k_a^{TPA,\ Fn} \times [TPA] \times ([Fn] - [TPA_B]) + k_d^{TPA_B} \times [TPA_B] \quad (3)$$

For example, Eq. 3 describes changes in TPA concentration due to three processes (fluxes): diffusion (the first term),

TABLE 1 Sensitivity of Lysis Propagation to Model Parameters

Parameter	Without Flow	With Flow	Mechanism
TPA	↑	–	More TPA drives faster lysis
PAI-1	↓	–	Less TPA slows lysis
D_{TPA}	↑	↑	Faster TPA propagation causes faster lysis

The up arrow (↑) clot lysis proceeds more efficiently (LAS increases) with parameter increase. The down arrow (↓) clot lysis proceeds less efficiently (LAS decreases) with parameter increase. The en-dash (–) parameter has no effect on clot lysis propagation (LAS does not change).

advection (the second term), and chemical reactions (the remaining terms in the second line).

These parameters show whether a certain type of change in the concentration of reagent j has an impact on spatial clot lysis.

$$R_j^S = \frac{LAS_{j^{ON}} - LAS_{j^{OFF}}}{LAS_{j^{ON}}}, \tag{4}$$

$$R_j^W = \frac{LFW_{j^{ON}} - LFW_{j^{OFF}}}{LFW_{j^{ON}}}. \tag{5}$$

Considering TPA fluxes, such as diffusion, we calculated LAS with the first term of Eq. 3 included in the model (LAS_{ON}) and LAS with the first term of Eq. 3 removed from the model (LAS_{OFF}), and based on these values, we obtained the R^S coefficient for TPA diffusion. For TPA advection, we performed calculations with and without the second term, and for TPA chemical flux, we performed calculations with and without terms in the second line of Eq. 3 (whereas the rest of the equations in the model remained unchanged).

The results of these simulations are shown in Tables 3, 4, 5, 6, and 7.

In Table 3, we show how the absence of each reagent changes the clot lysis process. As the absolute values of the necessity coefficients for the chemical reactions for α_2M and α_2AP are less than 0.05 (Table 4), the impact of changes in the α2M and α2AP concentrations is very low, so these can be neglected and their concentrations assumed to be constant. As a result, we can remove Eqs. S10 and S11 and substitute α_2M and α_2AP in Eqs. S4, S7, and S8 with constants α_2M_0 and α_2AP_0. This simplification of the original model demonstrates that general inhibitors (α_2M and α_2AP) are in excess, and their impact on spatial lysis can be expressed as first-order inhibition.

In Table 4, we show how the absence of the chemical flux that regulates certain reagent concentrations changes the clot lysis process. The absolute values of PgG-related reaction coefficients with and without flow are less than 0.05 for R^S and R^W (Table 4), so we can neglect the changes in the PgG concentration and treat it as a constant. Thus, we can remove S3 and replace PgG in all equations with its constant initial concentration PgG_0. Under the conditions of spatial clot lysis considered here, the depletion of PgG is negligible, whereas the necessity of PgG for spatial lysis is naturally critical ($R^S_{PgG} = 1$, $R^W_{PgG} = 1$).

In Tables 5 and 6, we show how the absence of the diffusional or advectional flux of a certain reagent changes the clot lysis process. Importantly, the absolute values of diffusional necessity coefficients for PgG, PgL, and Pn were lower than 0.05 (Table 5); thus, we can neglect the diffusion of all reagents except for TPA and PAI-1. This means that the local depletion of lysis factors has only a marginal effect on fibrin clot spatial dissolution. The same holds for advection because the absolute values of necessity coefficients for advection of PgG, PgL, and Pn are lower than 0.05 (Table 6). The impact of all these changes in the equations (step 1) is shown in Table 7. Here, to obtain the coefficient, we used the LAS (LFW) parameter calculated before changes

TABLE 2 Sensitivity of LFW to Model Parameters

Parameter	Without Flow	With Flow	Mechanism
Fn	↓	↓	More TPA bound, faster local lysis
α_2AP	↑	↑	More bound Pn inhibited, slower local lysis
TPA	–	↓	TPA transportation by flow makes local lysis faster
PgG	↓	↓	More Pn generated, faster local lysis
PAI-1	↓	↓	Narrower TPA distribution, narrower region of local lysis
$k_a^{TPA,\ Fn}$	↓	↓	More TPA bound, faster local lysis
$k_a^{PgG,\ Fn}$ ($k_d^{PgG_B}$)	↓(↑)	↓(↑)	More (less) Pn generated, faster (slower) local lysis
$k_{cat}^{Fn,\ Pn}$	↓	↓	Faster local lysis
$k_{cat}^{PgG_B,\ TPA_B}$	↓	↓	More Pn generated, faster local lysis
$k_i^{Pn_B,\ \alpha_2AP}$	↑	↑	More bound Pn inhibited, slower local lysis
D_{TPA}	↑	↑	Wider TPA distribution, wider region of local lysis
D_{PAI1}	↑	–	Wider region of PAI-1 depletion, wider TPA distribution, wider region of local lysis

The up arrow (↑) clot lysis occurs in a wider zone (LFW increases) with parameter increase. The down arrow (↓) clot lysis occurs in a narrower zone (LFW decreases) with parameter increase. The en-dash (–) parameter has no effect on area of clot lysis (LFW does not change).

TABLE 3 The Necessity Coefficients for Chemical Reagents

	$p = 0$ (No Flow)		$p = 100$ Pa	
Reagent	R^S	R^W	R^S	R^W
α_2M	0	−0.04261	6.38788E-4	0.00795
α_2AP	−0.13867	0.29255	−0.03356	0.28573
PAI-1	−0.5884	−1.5231	−0.31629	−0.53013
PgG	1	1	1	1
TPA	1	1	1	1

were complete (LAS_{ON}) and after changes were complete (LAS_{OFF}). After this reduction, we obtained a nine-equation model (Eqs. S13–S21).

Our simulations also demonstrate that the maximal achieved concentration of PgL is 10^{-11} mol/m^3, and the maximal concentration of its fibrin-bound form PgL_B is 10^{-8} mol/m^3. Because the main PgG activator is TPA, which activates fibrin-bound PgG ~500 times faster than it activates free PgG directly to Pn, we can neglect this intermediate formation in the reduced version of the model. Thus, we can remove these steps of Pn activation, making it straight from Pg to Pn. We thus remove Eqs. S15 and S17. These modifications (step 2 in Table 7) produce a seven-equation model (Eqs. S22–S28).

The maximal fibrin-bound plasmin Pn_B level achieved in our simulations is 2×10^{-6} mol/m^3 (2 nM). Because the fibrin clot is already formed before TPA addition, PgG is already bound to fibrin by the time of simulation onset, and only a fraction of PgG is cleaved; thus, only small changes in its concentration occur. Despite the relatively slow rate of plasmin(ogen) binding to fibrin, only small changes in the concentration of plasmin(ogen) bound to fibrin occur during spatial lysis. Thus, PgG_B is assumed to be in equilibrium with its free form, and the equation that describes changes in PgG_B concentration due to its binding with fibrin is replaced by

$$\frac{d[PgG_B]}{dt} = k_a^{PgG,\,Fn} \times [PgG_0] \times (2 \times [Fn] - [Pn_B] - [PgG_B]) - k_d^{PgG_B} \times [PgG_B] = 0, \quad (6)$$

with a quasistationary variable $PgG_B^{eq} = 2 \times PgG_0 \times [Fn]/(k_d^{PgG_B}/k_a^{PgG,Fn}) + PgG_0$. The term (2 × Fn-$Pn_B$) was also changed to 2 × Fn because the fibrin concentration was much larger than that of Pn bound to fibrin. This modification

TABLE 4 The Necessity Coefficients for Biochemical Reactions for Fibrin Clot Lysis

	$p = 0$ (No Flow)		$p = 100$ Pa	
Reagent	R^S	R^W	R^S	R^W
α_2M	0	−0.04261	0.00913	0.01272
α_2AP	0	0	−0.02571	−0.04443
PgG	0	−0.04261	−0.00392	0.04128
PAI-1	0.91018	0.43382	0.96783	0.77575
TPA	−0.7931	−1.91431	−0.39153	−0.67298

TABLE 5 The Necessity Coefficients for the Diffusion of Reagents for Fibrin Clot Lysis

	$p = 0$ (No Flow)		$p = 100$ Pa	
Reagent	R^S	R^W	R^S	R^W
PgG	0.00362	−0.03455	0.0052	0.00795
PgL	0	−0.04261	6.38788E-4	0.00795
Pn	0	0	−0.01761	0
PAI-1	−0.01371	0.15899	0	−0.02061
TPA	0.99417	0.91263	0.15897	0.41587
All factors except TPA	−0.00993	0.18563	−0.0029	−0.02061

(step 3 in Table 7) produces a model of six differential equations and one algebraic equation (Eqs. S29–S35).

Because TPA_B activates PgG_B 500 times faster than free TPA activates free PgG, the activation of free PgG can be disregarded, and because the Pn_B/Pn ratio inside the clot is ~10, free Pn can be removed from the model. This modification (step 4 in Table 7) leaves five differential equations (Eqs. 7, 8, 9, 10, 11, and 12). This reduction indicates that the activation of fibrin-bound PgG only is important for spatial clot lysis.

$$\frac{d[Fn]}{dt} = -k_{cat}^{Fn,Pn} \times [Pn_B], \quad (7)$$

$$\frac{d[Pn_B]}{dt} = -([Fn] > 0) \times \frac{[Pn_B]}{[Fn]} \times k_{cat}^{Fn,Pn} \times [Pn_B] + k_{cat}^{PgG_B,TPA_B} \times [TPA_B] \times PgG_B^{eq} - k_i^{Pn_B,\alpha_2AP} \times \alpha_2AP_0 \times [Pn_B], \quad (8)$$

$$\frac{\partial[TPA]}{\partial t} = D_{TPA} \times \frac{\partial^2[TPA]}{\partial x^2} - u \times \frac{\partial[TPA]}{\partial x} - k_a^{TPA,Fn} \times [TPA] \times ([Fn] - [TPA_B]) + k_d^{TPA_B} \times [TPA_B] - k_i^{TPA,PAI-1} \times [TPA] \times [PAI - 1], \quad (9)$$

$$\frac{d[TPA_B]}{dt} = k_a^{TPA,Fn} \times [TPA] \times ([Fn] - [TPA_B]) - k_d^{TPA_B} \times [TPA_B], \quad (10)$$

TABLE 6 The Necessity Coefficients for the Advection of Reagents for Fibrin Clot Lysis

	$p = 100$ Pa	
Reagent	R^S	R^W
PgG	−0.01533	−0.02856
PgL	−0.04268	−0.00792
Pn	6.38788E-4	0.00795
PAI-1	0.16253	0.45715
TPA	0.77004	0.33016
All factors except TPA	0.16024	0.44128

TABLE 7 The Necessity Coefficients for Model Reduction Steps for Fibrin Clot Lysis

	$p = 0$ (No Flow)		$p = 100$ Pa	
	R^S	R^W	R^S	R^W
Step 1	0.00362	0	−0.0746	−0.06507
Step 2	0.00362	−0.03455	0.00621	−0.04443
Step 3	−0.02758	0.00968	−0.00392	0.04923
Step 4	−0.02758	0.00968	−0.02051	0.03651

$$\frac{\partial[PAI-1]}{\partial t} = D_{PAI-1} \times \frac{\partial^2[PAI-1]}{\partial x^2} - u \times \frac{\partial[PAI-1]}{\partial x} - k_i^{TPA,PAI-1} \times [TPA] \times [PAI-1], \tag{11}$$

$$PgG_B^{eq} = \frac{2 \times PgG_0 \times [Fn]}{\frac{K_d^{PgG_B}}{K_a^{PgG,Fn}} + PgG_0}. \tag{12}$$

The reduction of the detailed model (12 PDEs) to a much smaller set (two PDEs, three ordinary differential equations, one constraint equation) underlines the main regulatory processes of spatial fibrin clot lysis: the diffusion of TPA into the clot and the activation of clot-bound PgG regulate lysis propagation.

In the presence or absence of flow, the reduced model of spatial clot lysis shows the same lysis progress as the detailed model (Fig. 2).

Analysis of the reduced model

To gain insight into the mechanisms of thrombolysis underlying the effects described above, such as the impact of TPA diffusion and PAI-1 concentration on LFW and lysis propagation, we analyzed the distribution of TPA within the clot during lysis (Fig. 3). The originally high TPA on the clot boundary did not last long because the clot boundary moved to the left with lysis, and TPA, because of diffusion, followed it with gradually decreasing concentration. Here, we show the free TPA concentration, as only its transportation defines lysis propagation. After 10 min, in the absence of flow, the TPA at the boundary of the solid clot and liquid plasma was more than 10 times lower than the TPA concentration outside the clot. We can see an increase in TPA concentration at the edge of the clot after 40 min of simulation, which occurs because of partial clot lysis: by this time, ~30% of the initial clot is dissolved, and its overall permeability increases; thus, more TPA can penetrate into it. If we look at the case of slower flow (10 Pa of hydrostatic pressure difference), less than 10% of the clot is dissolved by the end of the simulation, and the TPA concentration at the edge of the clot gradually decreases (Fig. S7). These results explain why PAI-1 can affect thrombolysis velocity significantly even when its concentration is much lower than that of TPA; at the edge of the diffusing TPA front, in the region of interest (lysis), the TPA concentration is much lower. In the presence of flow, this effect decreased because of additional TPA transport, and the difference was approximately threefold.

In agreement with the mechanism of PAI-1 action described above, PAI-1 inhibited lysis velocity and made the transition zone from solid clot to liquid (LFW) essentially narrower in a dose-dependent manner (Fig. 4). However, with increasing hydrostatic pressure difference, this effect diminishes. For simulations without flow, PAI-1 decelerates lysis and makes the front narrower by a factor of 3–4, notwithstanding its concentration being an order of magnitude lower than that of TPA; in the presence of 100 Pa pressure, its effects are less than twofold.

The decrease in the PAI-1 inhibitory effect on lysis under flow conditions can be explained by the following mechanism. TPA is inhibited by PAI-1 when the inhibitor concentration is greater than the TPA concentration. In the absence of flow, PAI-1 limits the zone of TPA penetration in the clot to the size of the LFW, whereas in the presence of flow, TPA penetrates farther into the clot (Fig. S8). Variation in PAI-1 concentration causes changes in the size of this zone, and in the absence of flow, this effect is greater, as the relative size of this zone is smaller.

Thrombolysis in the presence of collateral vessels

An important physical condition that can have an impact on the clot lysis process is the bypass of blood through the collateral vessel. To evaluate this effect, we performed a simulation of fibrin clot lysis in a 3D geometry for two values of hydrostatic pressure difference, 10 Pa (Figs. 5, 6, and 7) and 100 Pa (Figs. S9–S11). In the first case, TPA gradually penetrates into the clot, and fibrin also gradually lyses from the side of the TPA inlet. In the second case, TPA is rapidly pumped through the clot, and lysis proceeds in its entirety. This also explains why the LFW can increase with time, as shown in Fig. 4, *F* and *H*; it occurs when the clot is sufficiently lysed and the pressure difference becomes high enough to pump TPA through it.

We simulated clot lysis for three different vasculature surroundings: in the absence of collateral vessels, in the presence of collateral vessels with joint inlets and outlets, and in the presence of collateral vessels with joint inlets and separate outlets. The simulation geometry is shown in Fig. 5, *A–C*. The time course of fibrin dissolution is shown in Fig. 5, *D–F*. Here, we calculated the average fibrin concentration within the upper vessel (region shown with *blue* in Fig. 5, *A–C*). The time course of the average free TPA inside the upper vessel is shown in Fig. 5, *G–I*. The average flow velocity in the upper vessel and in the corresponding

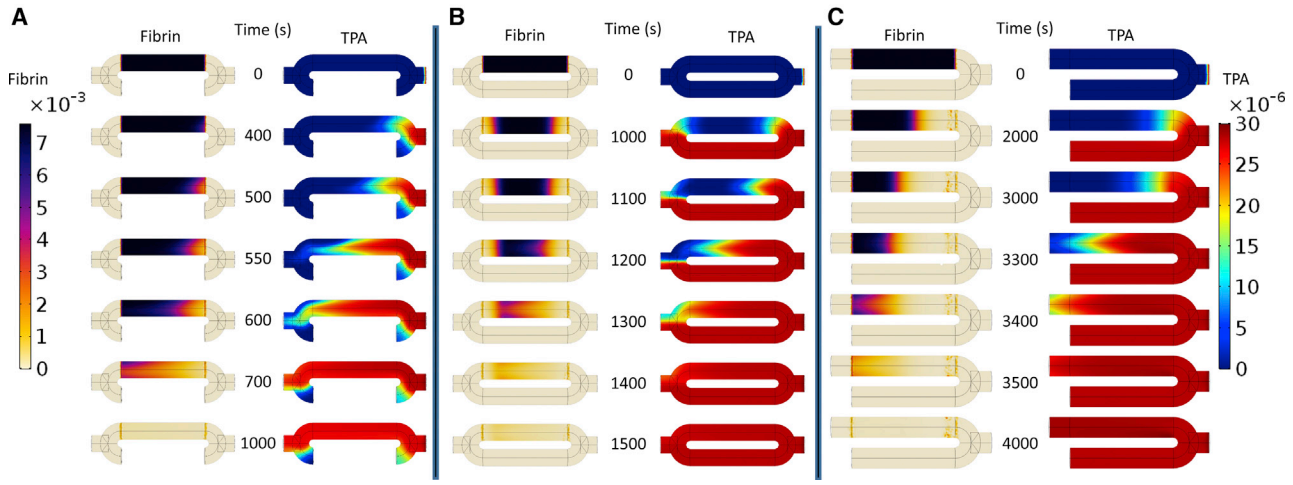

FIGURE 6 Spatial distribution of fibrin and free TPA in the chamber with a single channel (*A*), with collateral channels and a single exit (*B*) or in a chamber with collateral channels and separate exits (*C*). Simulations were performed in the 3D model. The hydrostatic pressure difference was 10 Pa, the clot permeability was 10^{-13} m^2, and the initial clot porosity was 0.99. To see this figure in color, go online.

region in the lower vessel (without clot) is shown in Fig. 5, *J–L*. The detailed spatial distribution of free TPA inside the clot and the time course of spatial clot dissolution are shown in Fig. 6. Here, the central section of the simulation area ($z = 0$) is shown. We can see how in the first stages, TPA slowly penetrates into the clot (Figs. 5, *G–I* and 6), which causes gradual clot dissolution (Figs. 5, *D–F* and 6), and when the clot size decreases, TPA can be pumped through it, and lysis of the remnant clot occurs rapidly. This process is accompanied by recanalization (Fig. 5, *J–L*), a rapid increase in the velocity of flow passing through the upper vessel.

We found that in the presence of collateral flow, lysis efficacy decreased because the TPA flux inside the clot was much lower than in the case of a single vessel. In the presence of a joint exit for collateral vessels (Fig. 5 *B*), the clot lysed from both ends (Fig. 6 *B*), which increased lysis efficacy compared with the case of separate exits for collateral vessels (Fig. 6 *C*), where lysis occurred only from one side (Fig. 6 *C*). In the absence of PAI-1 under low hydrostatic pressure difference conditions, the time of recanalization was almost insensitive to the collateral flow, whereas in the presence of PAI-1 at normal or doubled concentrations, the difference was drastic (Fig. 7). Increased PAI-1 levels in the case of collateral flows with separate exits caused an eightfold prolongation of recanalization time compared with the case of a single channel.

DISCUSSION

Our study focused on analysis of the spatial organization of thrombolysis in a reaction-diffusion-advection system with the goal of finding the relationship between the chemical architecture of the fibrinolytic cascade, physical conditions of the simulation area, transport processes during clot lysis, and roles played by different components in the spatial lysis dynamics. The following main conclusions can be drawn.

1) The key regulatory mechanism of clot lysis propagation is TPA transport, which is determined by TPA diffusion, advection, inhibition, and binding with fibrin inside the clot.
2) The diffusion and advection of PAI-1 regulate the width of the lysis front.
3) The inhibition of active enzymes can decrease the LFW if applied at the top of the cascade (inhibition of TPA by PAI-1) and increase it if applied at the bottom (inhibition of Pn by α2AP).
4) Thrombolysis is strongly regulated by the surrounding physical conditions, and the presence of collateral flow can drastically prolong the recanalization time.
5) Depending on the physical conditions, the initial PAI-1 level can have a minor effect on the recanalization time (when there is no collateral flow in the system, 200% of the PAI-1 normal concentration increases the recanalization time 1.4-fold compared with 0% of PAI-1) or a major effect when collateral vessels bypass the clotted vessels (200% of the PAI-1 normal concentration increases the recanalization time 4.2-fold compared with 0% of PAI-1).

These results suggest, to our knowledge, a novel, revised picture of thrombolysis from the biophysical, chemical engineering and nonlinear dynamics points of view. In this new model, the driving force of lysis front propagation is the slow variable represented by the concentration of a long-lived enzyme at the top of the fibrinolytic amplifier cascade (TPA). The pattern of clot lysis is completely determined by the interplay of TPA diffusion, advection, inhibition, and binding to fibrin, which, together, define the dynamics of its

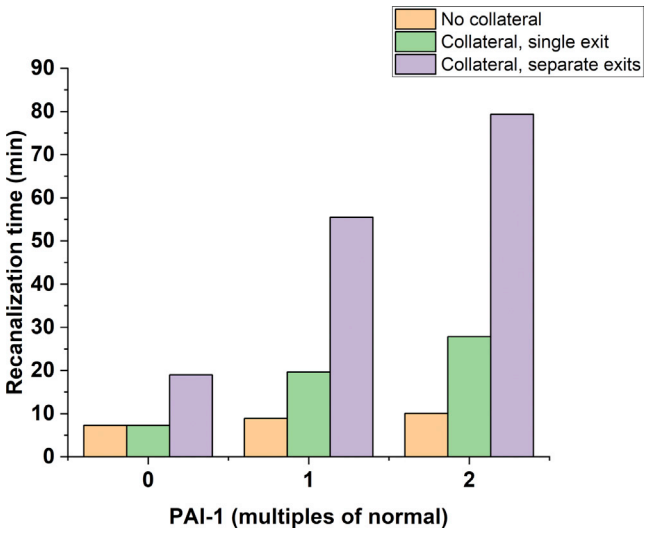

FIGURE 7 Recanalization time drastically depends on PAI-1 concentration in the presence of collateral vessels, especially with separate exits. Simulations were performed in the 3D model. The hydrostatic pressure difference was 10 Pa, the clot permeability was 10^{-13} m^2, and the initial clot porosity was 0.99. To see this figure in color, go online.

penetration into the clot and the pattern of thrombolysis. In contrast, the bottom enzyme of the cascade (Pn) is a rapid variable with high production and inhibition rates, and its diffusion is additionally rendered negligible by its tight binding to fibrin. From the chemical engineering point of view, this is strikingly similar to the organization of the blood coagulation cascade in which the enzymes factors IXa and XIa at the top are slow, well-diffusing variables (32,33) that drive clot propagation (34), whereas the enzymes factor Xa and thrombin in the bottom part of the cascade are fast variables with short effective diffusional distance that control the blood coagulation threshold (32,35).

In addition to diffusion, enzyme half-lives, regulated by their inhibition, play a significant role in the formation of the shape of the lysis front. A decrease in TPA half-life due to an increase in PAI-1 concentration or its inhibition constant causes decreases in both the LFW and the area of lysis propagation, whereas TPA diffusion has the opposite effect: its increase causes an increase in LFW and lysis propagation. These changes in the lysis process are brought by the overall spatial scaling of the upstream controlling variable. In contrast, a decrease in Pn half-life (predominantly, Pn is bound with fibrin) due to an increase in α_2AP concentration or an increase in the inhibition constant of Pn bound with fibrin by α_2AP causes an increase in LFW. This happens because of a decrease in the fibrin degradation rate (whereas an increase in the constant of fibrin degradation by Pn causes the LFW to decrease), and as the TPA distribution remains unchanged, fibrin in the solid state exists within a wider TPA concentration range.

Another mechanism we found in our study that can contribute to resistance to lysis therapy is the impact of surrounding vessels on the access of TPA to the thrombus that must be lysed. Collateral vessels can reroute TPA from the clotted vessel, causing sufficient delay in recanalization time. Depending on the geometry of collateral flows, the recanalization time may increase from twofold to sixfold.

Our model agrees with the previous models of spatial clot lysis (21,23) in terms of the importance of TPA permeation inside the clot but additionally includes the PAI-1 regulation of TPA distribution, which limits the lysis outcome. Despite the relatively low PAI-1 level (2 nM, ~10 times lower than the TPA concentration administered), it regulates TPA distribution at the very edge of the clot, where because of the limited transportation rate, the concentration of TPA is ~2–10 times lower than the administered concentration. The inhibitory effect of PAI-1 is greatly modified by the flow geometry. In the system with a single clotted channel, variation in PAI-1 concentration causes only mild changes in recanalization time, and even at PAI-1 twice the normal level, the recanalization time remains within 10 min. The bypassing flows cause a striking increase in recanalization time, which may be as high as 80 min.

This finding may indicate the reason for the relatively low success rate of thrombolytic therapy: elevated PAI-1 levels combined with the complex local geometry of the surrounding clotted vessel, with the possibility of bypassing flows, decrease the efficacy of spatial lysis and greatly prolong the recanalization time. These speculations can be confirmed by clinical data on the success rate of thrombolytic therapy. It is known that elevation of PAI-1 levels during patient admission reduces the chance of recanalization during TPA thrombolytic therapy (36). However, for thrombolytic therapy with tenecteplase, a longer-lived TPA variant with 80 times lower inhibition by PAI-1, it was shown that the PAI-1 level during patient admission did not correlate with the therapy outcome (37).

The model and the approach used in this study are, to our knowledge, novel compared to (22) because we employed necessity and sensitivity analysis to find the crucial reactions that regulated clot lysis propagation and LFW, as well as the impact of collateral flows on the overall lysis efficacy. One important assumption of this study is that the thrombus is preformed, and only its lysis is considered. As we showed earlier (18), different rules would function when clot formation and dissolution occur simultaneously. In particular, fibrinolysis itself would be driven by clot formation.

The following limitations of our simulations should be mentioned. Our approach can be described as "the most favorable conditions for lysis," as we wanted to estimate the maximal efficiency of lysis under certain conditions. We neglected the impact of thrombin-activatable fibrinolysis inhibitor (TAFI) on lysis. TAFI

reduces the amount of terminal lysines on the fibrin network, which are required for plasmin(ogen) and TPA binding. Thus, TAFI gradually downregulates lysis efficacy. In addition, TAFI is activated by the thrombin-thrombomodulin complex during the blood coagulation process; thus, correct incorporation of TAFI in the fibrinolysis model would require incorporation of the whole coagulation module, and this goal, although important, is beyond the scope of this research. We considered the clot to be uniform and the vessel completely occluded. No clot microstructure was considered during dissolution, and only one spatial scale (clot length) was used. Heterogeneous clot structure (fibrin, platelets, red blood cells), a complex geometry (branching cylindrical vessels) and nonuniform flow (pulsations, backward flow), and time- and space-dependent chemical conditions (secretion of reagents during lysis (13,38)) could further attenuate our results. The complex and contracted structure of the clot would decrease the overall lysis efficacy; thus, we considered a simple, uncontracted clot. Because of our "most favorable conditions for lysis" approach, we may speculate that any moves toward more realistic clots will decrease lysis efficiency. This could be the reason for the relatively low success rate of thrombolytic therapy. To improve the potential outcome of simulations in terms of understanding the clot lysis process, the next step could include the modeling of complex clot structure, which includes red blood cell distribution inside the clot, platelet aggregates and a contracted fibrin network. Realistic models of blood vessels where lysis occurs can also be helpful.

SUPPORTING MATERIAL

Supporting Material can be found online at https://doi.org/10.1016/j.bpj.2020.06.020.

AUTHOR CONTRIBUTIONS

A.M.S.: conceptualization, methodology, software, formal analysis, investigation, and writing for the original draft. B.C.: validation, data curation, and writing for review, editing, and funding acquisition. A.G.H.: formal analysis, and writing for review, editing, and funding acquisition. M.A.P.: conceptualization, methodology, project administration, supervision, and writing for review, editing, and funding acquisition.

ACKNOWLEDGMENTS

Model development was supported by grant 20-45-01014 from the Russian Science Foundation. A.G.H. and B.C. acknowledge support by the INSIST project (grant #777072 from the European Commission Horizon2020 program).

REFERENCES

1. Belyaev, A. V., J. L. Dunster, …, V. Volpert. 2018. Modeling thrombosis in silico: frontiers, challenges, unresolved problems and milestones. *Phys. Life Rev.* 26–27:57–95.
2. Panteleev, M. A., N. M. Dashkevich, and F. I. Ataullakhanov. 2015. Hemostasis and thrombosis beyond biochemistry: roles of geometry, flow and diffusion. *Thromb. Res.* 136:699–711.
3. Longstaff, C., and K. Kolev. 2015. Basic mechanisms and regulation of fibrinolysis. *J. Thromb. Haemost.* 13 (*Suppl 1*):S98–S105.
4. Sprengers, E. D., and C. Kluft. 1987. Plasminogen activator inhibitors. *Blood.* 69:381–387.
5. Foley, J. H. 2017. Plasmin(ogen) at the nexus of fibrinolysis, inflammation, and complement. *Semin. Thromb. Hemost.* 43:135–142.
6. Rånby, M. 1982. Studies on the kinetics of plasminogen activation by tissue plasminogen activator. *Biochim. Biophys. Acta.* 704:461–469.
7. Wiman, B., L. Boman, and D. Collen. 1978. On the kinetics of the reaction between human antiplasmin and a low-molecular-weight form of plasmin. *Eur. J. Biochem.* 87:143–146.
8. Liu, J. N., and V. Gurewich. 1991. A comparative study of the promotion of tissue plasminogen activator and pro-urokinase-induced plasminogen activation by fragments D and E-2 of fibrin. *J. Clin. Invest.* 88:2012–2017.
9. Thelwell, C., and C. Longstaff. 2007. The regulation by fibrinogen and fibrin of tissue plasminogen activator kinetics and inhibition by plasminogen activator inhibitor 1. *J. Thromb. Haemost.* 5:804–811.
10. Wehner, C., K. Janjić, and H. Agis. 2017. Relevance of the plasminogen system in physiology, pathology, and regeneration of oral tissues - from the perspective of dental specialties. *Arch. Oral Biol.* 74:136–145.
11. Medcalf, R. L. 2017. Fibrinolysis: from blood to the brain. *J. Thromb. Haemost.* 15:2089–2098.
12. Levin, E. G., U. Marzec, …, L. A. Harker. 1984. Thrombin stimulates tissue plasminogen activator release from cultured human endothelial cells. *J. Clin. Invest.* 74:1988–1995.
13. van den Eijnden-Schrauwen, Y., T. Kooistra, …, J. J. Emeis. 1995. Studies on the acute release of tissue-type plasminogen activator from human endothelial cells in vitro and in rats in vivo: evidence for a dynamic storage pool. *Blood.* 85:3510–3517.
14. Thiebaut, A. M., M. Gauberti, …, B. D. Roussel. 2018. The role of plasminogen activators in stroke treatment: fibrinolysis and beyond. *Lancet Neurol.* 17:1121–1132.
15. Wiyeh, A. B., E. A. Ochodo, …, B. M. Mayosi. 2018. A systematic review of the efficacy and safety of intrapericardial fibrinolysis in patients with pericardial effusion. *Int. J. Cardiol.* 250:223–228.
16. Fisher, M.; Stroke Therapy Academic Industry Roundtable. 2003. Recommendations for advancing development of acute stroke therapies: stroke therapy academic industry roundtable 3. *Stroke.* 34:1539–1546.
17. Coutts, S. B., E. Berge, …, M. W. Parsons. 2018. Tenecteplase for the treatment of acute ischemic stroke: a review of completed and ongoing randomized controlled trials. *Int. J. Stroke.* 13:885–892.
18. Zhalyalov, A. S., M. A. Panteleev, …, A. M. Shibeko. 2017. Co-ordinated spatial propagation of blood plasma clotting and fibrinolytic fronts. *PLoS One.* 12:e0180668.
19. Bannish, B. E., J. P. Keener, and A. L. Fogelson. 2014. Modelling fibrinolysis: a 3D stochastic multiscale model. *Math. Med. Biol.* 31:17–44.
20. Bannish, B. E., I. N. Chernysh, …, J. W. Weisel. 2017. Molecular and physical mechanisms of fibrinolysis and thrombolysis from mathematical modeling and experiments. *Sci. Rep.* 7:6914.
21. Diamond, S. L., and S. Anand. 1993. Inner clot diffusion and permeation during fibrinolysis. *Biophys. J.* 65:2622–2643.
22. Anand, S., and S. L. Diamond. 1996. Computer simulation of systemic circulation and clot lysis dynamics during thrombolytic therapy that accounts for inner clot transport and reaction. *Circulation.* 94:763–774.

23. Piebalgs, A., B. Gu, …, X. Y. Xu. 2018. Computational simulations of thrombolytic therapy in acute ischaemic stroke. *Sci. Rep.* 8:15810.

24. Carr, M. E., Jr., L. L. Shen, and J. Hermans. 1977. Mass-length ratio of fibrin fibers from gel permeation and light scattering. *Biopolymers.* 16:1–15.

25. Carr, M. E., Jr., and C. L. Hardin. 1987. Fibrin has larger pores when formed in the presence of erythrocytes. *Am. J. Physiol.* 253:H1069–H1073.

26. Blombäck, B., K. Carlsson, …, N. Aslund. 1989. Native fibrin gel networks observed by 3D microscopy, permeation and turbidity. *Biochim. Biophys. Acta.* 997:96–110.

27. Tanswell, P., U. Tebbe, …, E. Seifried. 1992. Pharmacokinetics and fibrin specificity of alteplase during accelerated infusions in acute myocardial infarction. *J. Am. Coll. Cardiol.* 19:1071–1075.

28. Seifried, E., P. Tanswell, …, A. Schmidt. 1989. Pharmacokinetics and haemostatic status during consecutive infusions of recombinant tissue-type plasminogen activator in patients with acute myocardial infarction. *Thromb. Haemost.* 61:497–501.

29. Auer, R. N. 2016. Histopathology of brain tissue response to stroke and injury. Stroke. Elsevier, pp. 47–59.

30. Wei, L., J. P. Erinjeri, …, T. A. Woolsey. 2001. Collateral growth and angiogenesis around cortical stroke. *Stroke.* 32:2179–2184.

31. Zhalyalov, A. S., A. N. Balandina, …, A. M. Shibeko. 2017. The overview of fibrinolysis system contemporary concepts and of its disorders diagnostic methods. *Pediatr. Hematol. Immunopathol.* 16:69–82.

32. Panteleev, M. A., A. N. Balandina, …, F. I. Ataullakhanov. 2010. Task-oriented modular decomposition of biological networks: trigger mechanism in blood coagulation. *Biophys. J.* 98:1751–1761.

33. Lipets, E., O. Vlasova, …, M. Panteleev. 2014. Circulating contact-pathway-activating microparticles together with factors IXa and XIa induce spontaneous clotting in plasma of hematology and cardiologic patients. *PLoS One.* 9:e87692.

34. Panteleev, M. A., M. V. Ovanesov, …, F. I. Ataullakhanov. 2006. Spatial propagation and localization of blood coagulation are regulated by intrinsic and protein C pathways, respectively. *Biophys. J.* 90:1489–1500.

35. Dashkevich, N. M., M. V. Ovanesov, …, F. I. Ataullakhanov. 2012. Thrombin activity propagates in space during blood coagulation as an excitation wave. *Biophys. J.* 103:2233–2240.

36. Ribo, M., J. Montaner, …, J. Alvarez-Sabín. 2004. Admission fibrinolytic profile predicts clot lysis resistance in stroke patients treated with tissue plasminogen activator. *Thromb. Haemost.* 91:1146–1151.

37. Huisse, M.-G., N. Ajzenberg, …, P. G. Steg. 2009. Microparticle-linked tissue factor activity and increased thrombin activity play a potential role in fibrinolysis failure in ST-segment elevation myocardial infarction. *Thromb. Haemost.* 101:734–740.

38. Brogren, H., L. Karlsson, …, S. Jern. 2004. Platelets synthesize large amounts of active plasminogen activator inhibitor 1. *Blood.* 104:3943–3948.

Biophysical Journal, Volume *119*

Supplemental Information

Redistribution of TPA Fluxes in the Presence of PAI-1 Regulates Spatial Thrombolysis

Alexey M. Shibeko, Bastien Chopard, Alfons G. Hoekstra, and Mikhail A. Panteleev

Table S1. List of acronyms

Fn – fibrin, the main component of the clot
PgG – glu-plasminogen, inactive precursor of plasmin
PgL – lys-plasminogen, partially activated form of plasminogen
Pn – plasmin, protease that cleaves fibrin
TPA – tissue plasminogen activator, activates plasmin
α_2AP – alpha-2-antiplasmin, inhibitor of plasmin
α_2M – alpha-2-macroglubulin, inhibitor of plasmin
PAI-1 – plasmin activator inhibitor 1, inhibitor of TPA

The subscript $_B$ is used to denote fibrin-bound reagents, e.g., PgG_B is glu-plasminogen bound with fibrin.
The subscript $_0$ is used to denote initial concentrations of reagents, i.e., α_2AP_0 is the initial concentration of α_2AP.

Table S2. Model parameters: initial conditions

1. Initial concentrations of model variables

Area x=0 to x=10		Area x=10 to x=20		Reference
Factor	Concentration, mol/m^3	Factor	Concentration, mol/m^3	
Fn	7.6e-3	Fn	0	(1)
PgL	0	PgL	0	
α_2AP	1.1e-3	α_2AP	1.1e-3	(2)
α_2M	3e-3	α_2M	3e-3	(3)
PAI-1	2e-6	PAI-1	2e-6	(2)
PgG	1.45e-3	PgG	2e-3	(2)
Pn	0	Pn	0	
TPA	0	TPA	1e-5 – 1e-3	(4–7)
PgG_B	0.55e-3	PgG_B	0	

Equations

$$\frac{\partial[TPA]}{\partial t} = D_{TPA}\cdot\frac{\partial^2[TPA]}{\partial x^2} - u\cdot\frac{\partial[TPA]}{\partial x} - k_i^{TPA,PAI\text{-}1}\cdot[TPA]\cdot[PAI\text{-}1] \quad \text{(S1)}$$

$$-k_a^{TPA,Fn}\cdot[TPA]\cdot([Fn]-[TPA_B]) + k_d^{TPA_B}\cdot[TPA_B]$$

$$\frac{\partial[TPA_B]}{\partial t} = k_a^{TPA,Fn}\cdot[TPA]\cdot([Fn]-[TPA_B]) - k_d^{TPA_B}\cdot[TPA_B] - ([Fn]>0)\cdot\frac{[TPA_B]}{[Fn]}\cdot k_{cat}^{Fn,Pn}\cdot[Pn_B] \quad \text{(S2)}$$

$$\frac{\partial[PgG]}{\partial t} = D_{PgG} \cdot \frac{\partial^2[PgG]}{\partial x^2} - u \cdot \frac{\partial[PgG]}{\partial x} - k_{cat}^{PgG,Pn} \cdot [Pn] \cdot [PgG] - \tag{S3}$$

$$k_a^{PgG,Fn} \cdot [PgG] \cdot (2 \cdot [Fn] - [Pn_B] - [PgG_B] - [PgL_B]) + k_d^{PgG_B} \cdot [PgG_B] - k_{cat}^{PgG,TPA} \cdot [TPA] \cdot [PgG]$$

$$\frac{\partial[PgL]}{\partial t} = D_{PgL} \cdot \frac{\partial^2[PgL]}{\partial x^2} - u \cdot \frac{\partial[PgL]}{\partial x} + k_{cat}^{PgG,Pn} \cdot [Pn] \cdot [PgG] - \tag{S4}$$

$$k_a^{PgL,Fn} \cdot [PgL] \cdot (2 \cdot [Fn] - [Pn_B] - [PgG_B] - [PgL_B]) + k_d^{PgL_B} \cdot [PgL_B] - k_{cat}^{PgL,TPA} \cdot [TPA] \cdot [PgL] -$$

$$k_i^{PgL,\alpha_2 AP} \cdot [\alpha_2 AP] \cdot [PgL]$$

$$\frac{\partial[PgG_B]}{\partial t} = k_a^{PgG,Fn} \cdot [PgG] \cdot (2 \cdot [Fn] - [Pn_B] - [PgG_B] - [PgL_B]) - k_d^{PgG_B} \cdot [PgG_B] -$$

$$k_{cat}^{PgG_B,Pn} \cdot [Pn] \cdot [PgG_B] - k_{cat}^{PgG_B,TPA_B} \cdot [TPA_B] \cdot [PgG_B] - ([Fn] > 0) \cdot \frac{[PgG_B]}{[Fn]} \cdot k_{cat}^{Fn,Pn} \cdot [Pn_B] \tag{S5}$$

$$\frac{\partial[PgL_B]}{\partial t} = k_a^{PgL,Fn} \cdot [PgL] \cdot (2 \cdot [Fn] - [Pn_B] - [PgG_B] - [PgL_B]) - k_d^{PgL_B} \cdot [PgL_B] +$$

$$k_{cat}^{PgG_B,Pn} \cdot [Pn] \cdot [PgG_B] - k_{cat}^{PgL_B,TPA_B} \cdot [TPA_B] \cdot [PgL_B] - ([Fn] > 0) \cdot \frac{[PgL_B]}{[Fn]} \cdot k_{cat}^{Fn,Pn} \cdot [Pn_B] \tag{S6}$$

$$-k_i^{PgL_B,\alpha_2 AP} \cdot [\alpha_2 AP] \cdot [PgL_B]$$

$$\frac{\partial[Pn]}{\partial t} = D_{Pn} \cdot \frac{\partial^2[Pn]}{\partial x^2} - u \cdot \frac{\partial[Pn]}{\partial x} + k_{cat}^{PgG,TPA} \cdot [TPA] \cdot [PgG] + k_{cat}^{PgL,TPA} \cdot [TPA] \cdot [PgL] - \tag{S7}$$

$$k_a^{Pn,Fn} \cdot [Pn] \cdot (2 \cdot [Fn] - [Pn_B] - [PgG_B] - [PgL_B]) + k_d^{Pn_B} \cdot [Pn_B] - k_i^{Pn,\alpha_2 AP} \cdot [\alpha_2 AP] \cdot [Pn] -$$

$$k_i^{Pn,\alpha_2 M} \cdot [\alpha_2 M] \cdot [Pn]$$

$$\frac{\partial[Pn_B]}{\partial t} = k_a^{Pn,Fn} \cdot [Pn] \cdot (2 \cdot [Fn] - [Pn_B] - [PgG_B] - [PgL_B]) - k_d^{Pn_B} \cdot [Pn_B]$$

$$-([Fn] > 0) \cdot \frac{[Pn_B]}{[Fn]} \cdot k_{cat}^{Fn,Pn} \cdot [Pn_B] + k_{cat}^{PgG_B,TPA_B} \cdot [TPA_B] \cdot [PgG_B] + k_{cat}^{PgL_B,TPA_B} \cdot [TPA_B] \cdot [PgL_B] - \tag{S8}$$

$$k_i^{Pn_B,\alpha_2 AP} \cdot [\alpha_2 AP] \cdot [Pn_B]$$

$$\frac{\partial[PAI\text{-}1]}{\partial t} = D_{PAI\text{-}1} \cdot \frac{\partial^2[PAI\text{-}1]}{\partial x^2} - u \cdot \frac{\partial[PAI\text{-}1]}{\partial x} - k_i^{TPA,PAI\text{-}1} \cdot [TPA] \cdot [PAI\text{-}1] \tag{S9}$$

$$\frac{\partial[\alpha_2 M]}{\partial t} = D_{\alpha_2 M} \cdot \frac{\partial^2[\alpha_2 M]}{\partial x^2} - u \cdot \frac{\partial[\alpha_2 M]}{\partial x} - k_i^{Pn,\alpha_2 M} \cdot [\alpha_2 M] \cdot [Pn] \tag{S10}$$

$$\frac{\partial[\alpha_2 AP]}{\partial t} = D_{\alpha_2 AP} \cdot \frac{\partial^2[\alpha_2 AP]}{\partial x^2} - u \cdot \frac{\partial[\alpha_2 AP]}{\partial x} - k_i^{Pn,\alpha_2 AP} \cdot [\alpha_2 AP] \cdot [Pn] - \tag{S11}$$

$$k_a^{Pn_B,\alpha_2AP}\cdot[\alpha_2AP]\cdot[Pn_B]-k_i^{PgL,\alpha_2AP}\cdot[\alpha_2AP]\cdot[PgL]$$

$$\frac{\partial[Fn]}{\partial t}=-k_{cat}^{Fn,Pn}\cdot[Pn_B] \quad \text{(S12)}$$

where u is the velocity of blood flow.
S1 TPA diffuses and advects; it is irreversibly inactivated by PAI-1 and reversibly binds free fibrin.
S2 TPA bound with fibrin dissolves due to fibrin degradation by plasmin. During clot lysis, fibrin is cleaved by plasmin, and part of TPA_B on it is removed from the clot with detached parts of fibrin. We assume that TPA_B is distributed evenly in the clot (within the local position), and the part of it that is released from the clot is proportional to its amount, which is described by the $\frac{[TPA_B]}{[Fn]}$ ratio.
S3 Glu-plasminogen diffuses and advects; it is activated to lys-plasminogen by plasmin, reversibly binds free fibrin, and is activated to plasmin by TPA.

According to (8), plasminogen binds near the end-to-end junction of two fibrin molecules, and TPA binds to γ-chain residues of fibrin. After lysis onset, C-terminal lysine residues of partially digested fibrin bind to lysine binding sites in certain kringle domains of plasminogen and TPA. In our model, we did not consider the size of fibrin clot structures, such as fibril formation, which also has an impact on the lysis process (9), or lysine residue exposure during clot lysis. Thus, we included only first-type binding sites, which are different for TPA and plasminogen. As a molecule of fibrin is a dimer of αβγ chains, it has two sites of binding for plasmin(ogen).

S4 Lys-plasminogen diffuses and advects; it is activated from glu-plasminogen by plasmin, reversibly binds free fibrin, is activated to plasmin by TPA and is inhibited by α_2AP.
S5 Glu-plasminogen bound with fibrin is activated to lys-plasminogen bound with fibrin by plasmin and to plasmin bound with fibrin by TPA bound with fibrin. Glu-plasminogen bound with fibrin dissolves due to fibrin degradation by plasmin.
S6 Lys-plasminogen bound with fibrin is activated from glu-plasminogen bound with fibrin by plasmin and is activated to plasmin by TPA bound with fibrin. Lys-plasminogen bound with fibrin dissolves due to fibrin degradation by plasmin and is inhibited by α_2AP.
S7 plasmin diffuses and advects; it is activated from glu- and lys-plasminogen by TPA, reversibly binds free fibrin and is inactivated by α_2AP and α_2M.
S8 plasmin bound with fibrin dissolves due to fibrin degradation by plasmin, is activated from glu- and lys-plasminogen bound with fibrin by TPA bound with fibrin and inhibited by α_2AP.
S9 PAI-1 diffuses and advects; it irreversibly binds with TPA.
S10 α_2M diffuses and advects; it irreversibly binds with plasmin.
S11 α_2AP diffuses and advects; it irreversibly binds with plasmin, plasmin bound with fibrin and lys-plasminogen.
S12 Fibrin dissolves. The rate of fibrin dissolution is proportional to the bound plasmin concentration, which depends on the fibrin concentration.

During model development, we also considered the following assumption.

The dissociation constant of the PgL interaction with antiplasmin is at least 10-fold higher than the Kd of PgG and antiplasmin (which is approximately 4 μM, almost 4 times higher than the antiplasmin concentration) (10). Thus, we neglected the PgG interaction with antiplasmin.

After step 1.

$$\frac{\partial[TPA]}{\partial t} = D_{TPA} \cdot \frac{\partial^2[TPA]}{\partial x^2} - u \cdot \frac{\partial[TPA]}{\partial x} - k_i^{TPA,PAI\text{-}1} \cdot [TPA] \cdot [PAI\text{-}1] \tag{S13}$$

$$- k_a^{TPA,Fn} \cdot [TPA] \cdot ([Fn] - [TPA_B]) + k_d^{TPA_B} \cdot [TPA_B]$$

$$\frac{d[TPA_B]}{dt} = k_a^{TPA,Fn} \cdot [TPA] \cdot ([Fn] - [TPA_B]) - k_d^{TPA_B} \cdot [TPA_B] - ([Fn] > 0) \cdot \frac{[TPA_B]}{[Fn]} \cdot k_{cat}^{Fn,Pn} \cdot [Pn_B] \tag{S14}$$

$$\frac{d[PgL]}{dt} = k_{cat}^{PgG,Pn} \cdot [Pn] \cdot PgG_0 - k_a^{PgL,Fn} \cdot [PgL] \cdot (2 \cdot [Fn] - [Pn_B] - [PgG_B] - [PgL_B]) \tag{S15}$$

$$+ k_d^{PgL_B} \cdot [PgL_B] - k_{cat}^{PgL,TPA} \cdot [TPA] \cdot [PgL] - k_i^{PgL,\alpha_2 AP} \cdot \alpha_2 AP_0 \cdot [PgL]$$

$$\frac{d[PgG_B]}{dt} = k_a^{PgG,Fn} \cdot PgG_0 \cdot (2 \cdot [Fn] - [Pn_B] - [PgG_B] - [PgL_B]) - k_d^{PgG_B} \cdot [PgG_B] -$$

$$k_{cat}^{PgG_B,Pn} \cdot [Pn] \cdot [PgG_B] - k_{cat}^{PgG_B,TPA_B} \cdot [TPA_B] \cdot [PgG_B] - ([Fn] > 0) \cdot \frac{[PgG_B]}{[Fn]} \cdot k_{cat}^{Fn,Pn} \cdot [Pn_B] \tag{S16}$$

$$\frac{d[PgL_B]}{dt} = k_a^{PgL,Fn} \cdot [PgL] \cdot (2 \cdot [Fn] - [Pn_B] - [PgG_B] - [PgL_B]) - k_d^{PgL_B} \cdot [PgL_B] +$$

$$k_{cat}^{PgG_B,Pn} \cdot [Pn] \cdot [PgG_B] - k_{cat}^{PgL_B,TPA_B} \cdot [TPA_B] \cdot [PgL_B] - ([Fn] > 0) \cdot \frac{[PgL_B]}{[Fn]} \cdot k_{cat}^{Fn,Pn} \cdot [Pn_B] \tag{S17}$$

$$- k_i^{PgL_B,\alpha_2 AP} \cdot \alpha_2 AP_0 \cdot [PgL_B]$$

$$\frac{d[Pn]}{dt} = k_{cat}^{PgG,TPA} \cdot [TPA] \cdot PgG_0 + k_{cat}^{PgL,TPA} \cdot [TPA] \cdot [PgL] - \tag{S18}$$

$$k_a^{Pn,Fn} \cdot [Pn] \cdot (2 \cdot [Fn] - [Pn_B] - [PgG_B] - [PgL_B]) + k_d^{Pn_B} \cdot [Pn_B] - k_i^{Pn,\alpha_2 AP} \cdot \alpha_2 AP_0 \cdot [Pn] -$$

$$k_i^{Pn,\alpha_2 M} \cdot \alpha_2 M_0 \cdot [Pn]$$

$$\frac{d[Pn_B]}{dt} = k_a^{Pn,Fn} \cdot [Pn] \cdot (2 \cdot [Fn] - [Pn_B] - [PgG_B] - [PgL_B]) - k_d^{Pn_B} \cdot [Pn_B]$$

$$- ([Fn] > 0) \cdot \frac{[Pn_B]}{[Fn]} \cdot k_{cat}^{Fn,Pn} \cdot [Pn_B] + k_{cat}^{PgG_B,TPA_B} \cdot [TPA_B] \cdot [PgG_B] + k_{cat}^{PgL_B,TPA_B} \cdot [TPA_B] \cdot [PgL_B] - \tag{S19}$$

$$k_i^{Pn_B,\alpha_2 AP} \cdot \alpha_2 AP_0 \cdot [Pn_B]$$

$$\frac{\partial[PAI\text{-}1]}{\partial t} = D_{PAI\text{-}1} \cdot \frac{\partial^2[PAI\text{-}1]}{\partial x^2} - u \cdot \frac{\partial[PAI\text{-}1]}{\partial x} - k_i^{TPA,PAI\text{-}1} \cdot [TPA] \cdot [PAI\text{-}1] \tag{S20}$$

$$\frac{d[Fn]}{dt} = - k_{cat}^{Fn,Pn} \cdot [Pn_B] \tag{S21}$$

S3 was removed, and PgG consumption was neglected.
S10 was removed, and α_2M consumption was neglected.

S11 was removed, and α_2AP consumption was neglected.
Diffusion and advection terms for all species except for TPA and PAI-1 were removed.

S13 is S1, no changes were made.
S14 is S2, no changes were made.
S15 is S4, PgG changed to PgG_0 and α_2AP changed to α_2AP_0.
S16 is S5, PgG changed to PgG_0.
S17 is S6, α_2AP changed to α_2AP_0.
S18 is S7, PgG changed to PgG_0, α_2AP changed to α_2AP_0 and α_2M changed to α_2M_0.
S19 is S8, α_2AP changed to α_2AP_0.
S20 is S9, no changes were made.
S21 is S12, no changes were made.

After step 2

$$\frac{\partial[TPA]}{\partial t} = D_{TPA}\cdot\frac{\partial^2[TPA]}{\partial x^2} - u\cdot\frac{\partial[TPA]}{\partial x} - k_i^{TPA,PAI\text{-}1}\cdot[TPA]\cdot[PAI\text{-}1] \quad \text{(S22)}$$

$$- k_a^{TPA,Fn}\cdot[TPA]\cdot([Fn]-[TPA_B]) + k_d^{TPA_B}\cdot[TPA_B]$$

$$\frac{d[TPA_B]}{dt} = k_a^{TPA,Fn}\cdot[TPA]\cdot([Fn]-[TPA_B]) - k_d^{TPA_B}\cdot[TPA_B] - ([Fn]>0)\cdot\frac{[TPA_B]}{[Fn]}\cdot k_{cat}^{Fn,Pn}\cdot[Pn_B] \quad \text{(S23)}$$

$$\frac{d[PgG_B]}{dt} = k_a^{PgG,Fn}\cdot PgG_0\cdot(2\cdot[Fn]-[Pn_B]-[PgG_B]) - k_d^{PgG_B}\cdot[PgG_B] - k_{cat}^{PgG_B,Pn}\cdot[Pn]\cdot[PgG_B] -$$

$$k_{cat}^{PgG_B,TPA_B}\cdot[TPA_B]\cdot[PgG_B] - ([Fn]>0)\cdot\frac{[PgG_B]}{[Fn]}\cdot k_{cat}^{Fn,Pn}\cdot[Pn_B] \quad \text{(S24)}$$

$$\frac{d[Pn]}{dt} = k_{cat}^{PgG,TPA}\cdot[TPA]\cdot PgG_0 - \quad \text{(S25)}$$

$$k_a^{Pn,Fn}\cdot[Pn]\cdot(2\cdot[Fn]-[Pn_B]-[PgG_B]) + k_d^{Pn_B}\cdot[Pn_B] - k_i^{Pn,\alpha_2AP}\cdot\alpha_2AP_0\cdot[Pn]$$

$$- k_i^{Pn,\alpha_2M}\cdot\alpha_2M_0\cdot[Pn]$$

$$\frac{d[Pn_B]}{dt} = k_a^{Pn,Fn}\cdot[Pn]\cdot(2\cdot[Fn]-[Pn_B]-[PgG_B]) - k_d^{Pn_B}\cdot[Pn_B] - ([Fn]>0)\cdot\frac{[Pn_B]}{[Fn]}\cdot k_{cat}^{Fn,Pn}\cdot[Pn_B] +$$

$$k_{cat}^{PgG_B,TPA_B}\cdot[TPA_B]\cdot[PgG_B] - k_i^{Pn_B,\alpha_2AP}\cdot\alpha_2AP_0\cdot[Pn_B] \quad \text{(S26)}$$

$$\frac{\partial[PAI\text{-}1]}{\partial t} = D_{PAI\text{-}1}\cdot\frac{\partial^2[PAI\text{-}1]}{\partial x^2} - u\cdot\frac{\partial[PAI\text{-}1]}{\partial x} - k_i^{TPA,PAI\text{-}1}\cdot[TPA]\cdot[PAI\text{-}1] \quad \text{(S27)}$$

$$\frac{d[Fn]}{dt} = - k_{cat}^{Fn,Pn}\cdot[Pn_B] \quad \text{(S28)}$$

S15 and S17 were removed. As PgL and PgL_B concentrations were below 0.01 nM, we neglected this intermediate formation.

S22 is S13, no changes were made.
S23 is S14, no changes were made.
S24 is S16, PgL_B term was removed.
S25 is S18, PgL and PgL_B terms were removed.
S26 is S19, PgL_B terms were removed.
S27 is S20, no changes were made.
S28 is S21, no changes were made.

After step 3

$$\frac{\partial[TPA]}{\partial t} = D_{TPA} \cdot \frac{\partial^2[TPA]}{\partial x^2} - u \cdot \frac{\partial[TPA]}{\partial x} - k_i^{TPA,PAI\text{-}1} \cdot [TPA] \cdot [PAI\text{-}1] \tag{S29}$$

$$- k_a^{TPA,Fn} \cdot [TPA] \cdot ([Fn] - [TPA_B]) + k_d^{TPA_B} \cdot [TPA_B]$$

$$\frac{d[TPA_B]}{dt} = k_a^{TPA,Fn} \cdot [TPA] \cdot ([Fn] - [TPA_B]) - k_d^{TPA_B} \cdot [TPA_B] - ([Fn] > 0) \cdot \frac{[TPA_B]}{[Fn]} \cdot k_{cat}^{Fn,Pn} \cdot [Pn_B] \tag{S30}$$

$$\frac{d[Pn]}{dt} = k_{cat}^{PgG,TPA} \cdot [TPA] \cdot PgG_0 - \tag{S31}$$

$$k_a^{Pn,Fn} \cdot [Pn] \cdot (2 \cdot [Fn] - [PgG_B^{eq}]) + k_d^{Pn_B} \cdot [Pn_B] - k_i^{Pn,\alpha_2 AP} \cdot \alpha_2 AP_0 \cdot [Pn] - k_i^{Pn,\alpha_2 M} \cdot \alpha_2 M_0 \cdot [Pn]$$

$$\frac{d[Pn_B]}{dt} = k_a^{Pn,Fn} \cdot [Pn] \cdot (2 \cdot [Fn] - [PgG_B^{eq}]) - k_d^{Pn_B} \cdot [Pn_B] - ([Fn] > 0) \cdot \frac{[Pn_B]}{[Fn]} \cdot k_{cat}^{Fn,Pn} \cdot [Pn_B] +$$

$$k_{cat}^{PgG_B,TPA_B} \cdot [TPA_B] \cdot [PgG_B^{eq}] - k_i^{Pn_B,\alpha_2 AP} \cdot \alpha_2 AP_0 \cdot [Pn_B] \tag{S32}$$

$$\frac{\partial[PAI\text{-}1]}{\partial t} = D_{PAI-1} \cdot \frac{\partial^2[PAI\text{-}1]}{\partial x^2} - u \cdot \frac{\partial[PAI\text{-}1]}{\partial x} - k_i^{TPA,PAI\text{-}1} \cdot [TPA] \cdot [PAI\text{-}1] \tag{S33}$$

$$\frac{\partial[Fn]}{\partial t} = - k_{cat}^{Fn,Pn} \cdot [Pn_B] \tag{S34}$$

$$PgG_B^{eq} = \frac{2 \cdot PgG_0 \cdot [Fn]}{\frac{K_d^{PgG_B}}{K_a^{PgG,Fn}} + PgG_0} \tag{S35}$$

We replaced PgG_B with a quasistationary variable, PgG_B^{eq}.

S29 is S22, no changes were made.
S30 is S23, no changes were made.
S31 is S25, PgG_B changed to PgG_B^{eq}.
S32 is S26, PgG_B changed to PgG_B^{eq}.
S33 is S27, no changes were made.
S34 is S28, no changes were made.

S35 replaces S24.

After step 4 (final variant)

$$\frac{d[Fn]}{dt} = -k_{cat}^{Fn,Pn} \cdot [Pn_B] \quad \text{(S36)}$$

$$\frac{d[Pn_B]}{dt} = -([Fn] > 0) \cdot \frac{[Pn_B]}{[Fn]} \cdot k_{cat}^{Fn,Pn} \cdot [Pn_B] + k_{cat}^{PgG_B,TPA_B} \cdot [TPA_B] \cdot PgG_B^{\ eq} - k_i^{Pn_B,\alpha_2 AP} \cdot \alpha_2 AP_0 \cdot [Pn_B] \quad \text{(S37)}$$

$$\frac{\partial [TPA]}{\partial t} = D_{TPA} \cdot \frac{\partial^2 [TPA]}{\partial x^2} - u \cdot \frac{\partial [TPA]}{\partial x} - k_a^{TPA,Fn} \cdot [TPA] \cdot ([Fn] - [TPA_B]) \quad \text{(S38)}$$
$$+ k_d^{TPA_B} \cdot [TPA_B] - k_i^{TPA,PAI\text{-}1} \cdot [TPA] \cdot [PAI\text{-}1]$$

$$\frac{d[TPA_B]}{dt} = k_a^{TPA,Fn} \cdot [TPA] \cdot ([Fn] - [TPA_B]) - k_d^{TPA_B} \cdot [TPA_B] \ -([Fn] > 0) \cdot \frac{[TPA_B]}{[Fn]} \cdot k_{cat}^{Fn,Pn} \cdot [Pn_B] \quad \text{(S39)}$$

$$\frac{\partial [PAI\text{-}1]}{\partial t} = D_{PAI\text{-}1} \cdot \frac{\partial^2 [PAI\text{-}1]}{\partial x^2} - u \cdot \frac{\partial [PAI\text{-}1]}{\partial x} - k_i^{TPA,PAI\text{-}1} \cdot [TPA] \cdot [PAI\text{-}1] \quad \text{(S40)}$$

$$PgG_B^{\ eq} = \frac{2 \cdot PgG_0 \cdot [Fn]}{\frac{K_d^{PgG_B}}{K_a^{PgG,Fn}} + PgG_0} \quad \text{(S41)}$$

TPA_B activates PgG_B 500 times faster than free TPA activates free Pg; thus, the activation of free plasminogen can be neglected, and the PnB/Pn ratio inside the clot is approximately 10. Therefore, we removed free plasmin (Pn) from the model.

S31 was removed.
S36 is S34, no changes were made.
S37 is S32, Pn terms were removed.
S38 is S29, no changes were made.
S39 is S30, no changes were made.
S40 is S33, no changes were made.
S41 is S35, no changes were made.

Flow module

$$\frac{\partial}{\partial t}(\varepsilon \cdot \rho) + \vec{\nabla} \cdot (\rho \cdot \vec{u}) = Q \quad \text{(S42)}$$

$$\vec{u} = -\frac{\kappa}{\mu} \vec{\nabla} p \quad \text{(S43)}$$

Here, $\varepsilon = 1 - 0.01 \cdot \frac{Fn}{Fn_0}$ is clot porosity, which was 0.99 for intact clot and 1 for completely dissolved clot.

$\rho = 1020 \frac{kg}{m^3}$ - blood plasma density.

$\mu = 0.0011 Pa \cdot s$ - blood plasma viscosity.

$\kappa = 10^{-14} - 10^{-12} m^2$ - fibrin clot permeability.

$p = 0 - 1000 Pa$ - pressure difference within the area boundaries.

The gradient operator means derivative with respect to x in the 1D case and derivative with respect to x, y, and z in the 3D case.

$\vec{u}$ – flow velocity. In the 1D case, we used the notation u for the flow velocity. In the 3D case, we used the notations u_x, u_y and u_z for the x, y and z components of the flow velocity.

Q – total discharge of blood plasma, which can be calculated from equations S42 and S43.

3D model of clot lysis

$$\frac{d[Fn]}{dt} = -k_{cat}^{Fn,Pn} \cdot [Pn_B] \tag{S44}$$

$$\frac{d[Pn_B]}{dt} = -([Fn] > 0) \cdot \frac{[Pn_B]}{[Fn]} \cdot k_{cat}^{Fn,Pn} \cdot [Pn_B] + k_{cat}^{PgG_B,TPA_B} \cdot [TPA_B] \cdot PgG_B^{\ eq} - k_i^{Pn_B,\alpha_2 AP} \cdot \alpha_2 AP_0 \cdot [Pn_B] \tag{S45}$$

$$\frac{\partial [TPA]}{\partial t} = D_{TPA} \cdot \left(\frac{\partial^2 [TPA]}{\partial x^2} + \frac{\partial^2 [TPA]}{\partial y^2} + \frac{\partial^2 [TPA]}{\partial z^2} \right) - u_x \cdot \frac{\partial [TPA]}{\partial x} - u_y \cdot \frac{\partial [TPA]}{\partial y} - u_z \cdot \frac{\partial [TPA]}{\partial z} \tag{S46}$$

$$-k_a^{TPA,Fn} \cdot [TPA] \cdot ([Fn] - [TPA_B]) + k_d^{TPA_B} \cdot [TPA_B] - k_i^{TPA,PAI\text{-}1} \cdot [TPA] \cdot [PAI\text{-}1]$$

$$\frac{d[TPA_B]}{dt} = k_a^{TPA,Fn} \cdot [TPA] \cdot ([Fn] - [TPA_B]) - k_d^{TPA_B} \cdot [TPA_B] \ -([Fn] > 0) \cdot \frac{[TPA_B]}{[Fn]} \cdot k_{cat}^{Fn,Pn} \cdot [Pn_B] \tag{S47}$$

$$\frac{\partial [PAI\text{-}1]}{\partial t} = D_{PAI\text{-}1} \cdot \left(\frac{\partial^2 [PAI\text{-}1]}{\partial x^2} + \frac{\partial^2 [PAI\text{-}1]}{\partial y^2} + \frac{\partial^2 [PAI\text{-}1]}{\partial z^2} \right) \tag{S48}$$

$$-u_x \cdot \frac{\partial [PAI\text{-}1]}{\partial x} - u_y \cdot \frac{\partial [PAI\text{-}1]}{\partial y} - u_z \cdot \frac{\partial [PAI\text{-}1]}{\partial z} - k_i^{TPA,PAI\text{-}1} \cdot [TPA] \cdot [PAI\text{-}1]$$

$$PgG_B^{\ eq} = \frac{2 \cdot PgG_0 \cdot [Fn]}{\frac{K_d^{PgG_B}}{K_a^{PgG,Fn}} + PgG_0} \tag{S49}$$

Table S3. Constants

Notation	Value	Reference
$k_i^{TPA,PAI\text{-}1}$	$2.5 \cdot 10^4 \ \frac{m^3}{mol \cdot s}$	(11)*
$k_a^{TPA,Fn}$	$0.115 \ \frac{m^3}{mol \cdot s}$	(12)
$k_d^{TPA_B}$	$6.67 \cdot 10^{-5} \ \frac{1}{s}$	(12)
$k_{cat}^{PgG,Pn}$	$5.67 \cdot 10^{-2} \ \frac{m^3}{mol \cdot s}$	(13)
$k_a^{PgG,Fn}$	$0.108 \ \frac{m^3}{mol \cdot s}$	(14)

$k_d^{PgG_B}$	$4.2 \cdot 10^{-3} \frac{1}{s}$	(14)
$k_{cat}^{PgG,TPA}$	$0.668 \ \frac{m^3}{mol \cdot s}$	(15)*
$k_a^{PgL,Fn}$	$0.108 \ \frac{m^3}{mol \cdot s}$	(14)
$k_d^{PgL_B}$	$5 \cdot 10^{-5} \frac{1}{s}$	(14)
$k_{cat}^{PgL,TPA}$	$9 \ \frac{m^3}{mol \cdot s}$	(15)*
$k_i^{PgL,\alpha_2 AP}$	$1000 \ \frac{m^3}{mol \cdot s}$	(16)
$k_{cat}^{PgG_B,Pn}$	$2.27 \ \frac{m^3}{mol \cdot s}$	(13)
$k_{cat}^{PgG_B,TPA_B}$	$333.3 \ \frac{m^3}{mol \cdot s}$	(15)*
$k_{cat}^{PgL_B,TPA_B}$	$5340 \ \frac{m^3}{mol \cdot s}$	(15)*
$k_a^{Pn,Fn}$	$0.109 \ \frac{m^3}{mol \cdot s}$	(17)
$k_d^{Pn_B}$	$5 \cdot 10^{-5} \frac{1}{s}$	(17)
$k_i^{Pn,\alpha_2 AP}$	$4.3 \cdot 10^3 \frac{m^3}{mol \cdot s}$	(18)
$k_i^{Pn,\alpha_2 M}$	$300 \ \frac{m^3}{mol \cdot s}$	(12)
$k_{cat}^{Fn,Pn}$	$5 \ \frac{1}{s}$ ¶	(19)
$k_i^{Pn_B,\alpha_2 AP}$	$10.8 \ \frac{m^3}{mol \cdot s}$	(18)
$k_i^{PgL_B,\alpha_2 AP}$	$10.8 \ \frac{m^3}{mol \cdot s}$	(18)*

* estimated value.

¶ - this value was increased 10 times to better fit the experimental data in work (20).

Table S4. Model parameters: diffusion coefficients

Model variable	M_r	Diffusion coefficient*, m^2/s
PgG	92,000	2.8e-11
PgL	92,000	2.8e-11
Pn	85,000	2.9e-11
TPA	68,000	3.3e-11
PAI-1	52,000	3.5e-11
α_2M	725,000	1e-11
α_2AP	70,000	3.3e-11

* The values of diffusion coefficients were estimated on the basis of the molecular weights of the components, using data from (21).

Sensitivity analysis

Sensitivity analysis was performed as described in (22).

To estimate system sensitivity to perturbations in parameters such as initial concentration, association/dissociation constants, catalytic or inhibition constants, we used sensitivity coefficients, which describe how the characteristics describing system behavior, LAS and LFW, depend on the variation in parameter *p*: parameter *p* was increased/decreased by the value δ, while the remaining parameters were fixed.

$$C^S = \frac{\frac{\Delta LAS}{LAS}}{\frac{\Delta p}{p}} \tag{S50}$$

Here, $\Delta LAS / LAS$ is the dimensionless change in LAS,

$$\Delta LAS = LAS\big|_{p=p_0+\delta} - LAS\big|_{p=p_0-\delta} \tag{S51}$$

$$LAS = LAS\big|_{p=p_0} \tag{S52}$$

$\Delta p / p = \frac{(p_0+\delta)-(p_0-\delta)}{p_0} = \frac{2\delta}{p_0}$ is the dimensionless change in p (S53)

If we change parameter *p* by value *i%* of p_0, we obtain the following formula:

$$C_i^S = \frac{LAS_{(100+i)\%} - LAS_{(100-i)\%}}{LAS_{100\%} \cdot 2 \cdot i \cdot 0.01} \tag{S54}$$

The same is true for the C^W coefficient.

We used different values of *i* (from 1 up to 10) to see how the system's sensitivity depends on it. For small values of *i* (up to 3), we obtained different sensitivity coefficients than for greater values, probably due to restrictions in simulations related to finite mesh size (the changes in LAS and LFW were too small to register them using the chosen mesh). However, for i>3, the sensitivity did not change with increasing i.

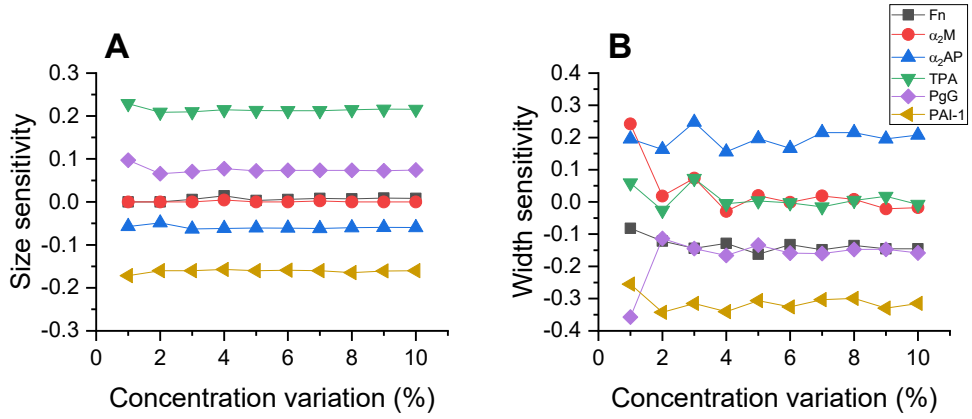

Fig. S1. Sensitivity of lysis area size (A) and lysis front width (B) to the variation of reagent initial concentration. The initial TPA concentration was 100 nM. Simulations were performed in the absence of flow.

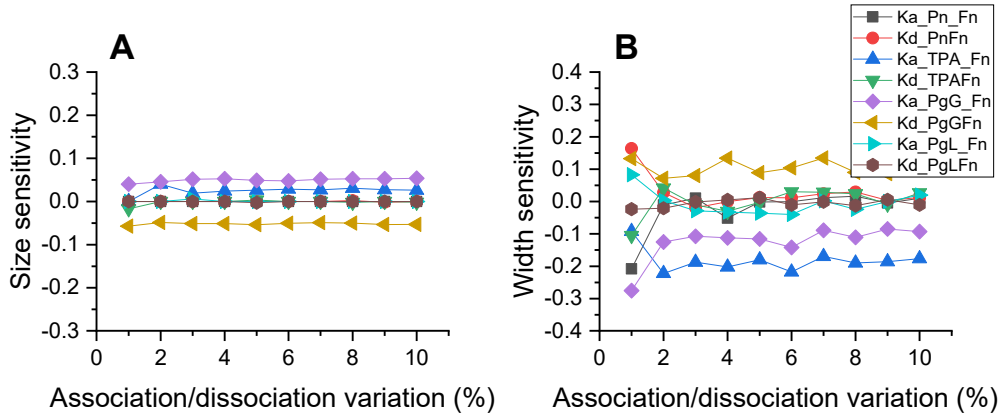

Fig. S2. Sensitivity of lysis area size (A) and lysis front width (B) for the variation in association/dissociation rate constants. The initial TPA concentration was 100 nM. Simulations were performed in the absence of flow.

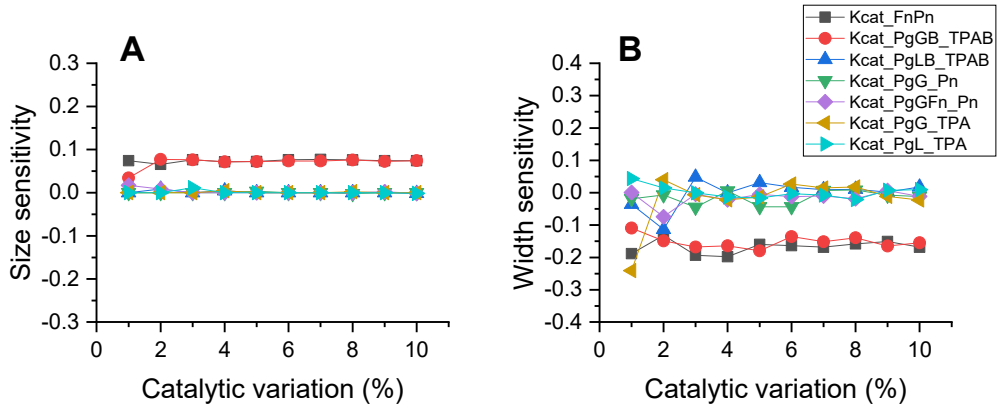

Fig. S3. Sensitivity of lysis area size (A) and lysis front width (B) to the variation in catalytic rate constants. The initial TPA concentration was 100 nM. Simulations were performed in the absence of flow.

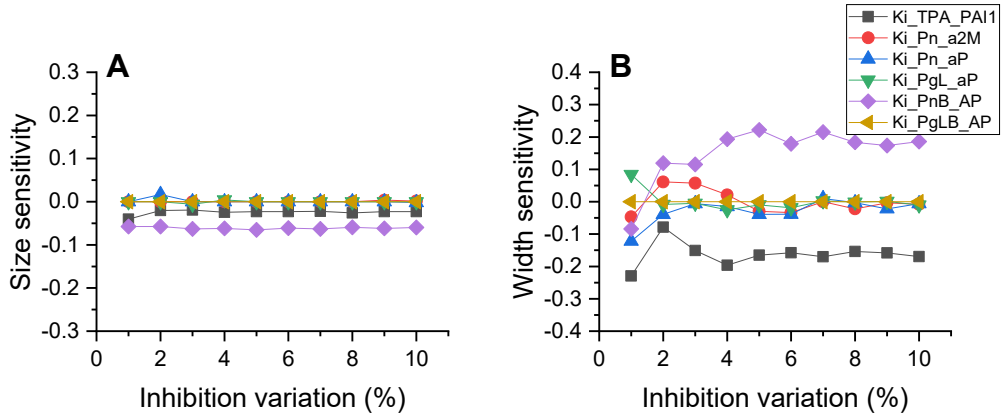

Fig. S4. Sensitivity of lysis area size (A) and lysis front width (B) to the variation in inhibition rate constants. The initial TPA concentration was 100 nM. Simulations were performed in the absence of flow.

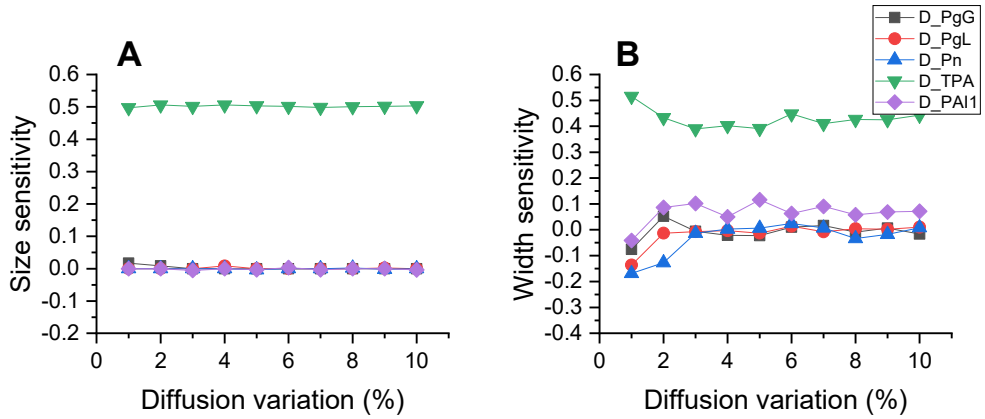

Fig. S5. Sensitivity of lysis area size (A) and lysis front width (B) to the variation in diffusion coefficients. The initial TPA concentration was 100 nM. Simulations were performed in the absence of flow.

Table S5. The values of C^S and C^W obtained for a range of TPA concentrations in the absence of flow.

	TPA 10 nM		TPA 100 nM		TPA 1000 nM	
	C^S 5%	**C^W 5%**	**C^S 5%**	**C^W 5%**	**C^S 5%**	**C^W 5%**
Fn	0.05352	**-0.15966**	0.00343	**-0.16249**	0.00795	**-0.13373**
α_2M	0	0.04507	0	0.01932	0	-0.01102
α_2AP	**-0.1338**	**0.13173**	-0.06062	**0.19654**	-0.03974	**0.21927**
TPA	**0.70377**	0.03871	**0.21273**	0.00308	**0.11571**	-0.01843
PgG	**0.14182**	**-0.12991**	0.07206	**-0.13374**	0.04991	**-0.16927**
PAI-1	**-0.66096**	**-0.38972**	**-0.16012**	**-0.30649**	-0.07947	**-0.27436**
--	--	--	--	--	--	--
$k_a^{Pn,Fn}$	0	0.03284	0	-0.00149	0	0.00218
$k_d^{Pn_B}$	0	0.00462	0	0.01223	0	0.00399
$k_a^{TPA,Fn}$	0.08831	**-0.09746**	0.02631	**-0.18031**	0.02162	**-0.18608**
$k_d^{TPA_B}$	-0.0107	0.09572	0.00343	-0.00279	0	-0.01083
$k_a^{PgG,Fn}$	0.10704	**-0.14821**	0.04918	**-0.11563**	0.03401	**-0.13524**
$k_d^{PgG_B}$	-0.10704	**0.1093**	-0.05376	**0.08913**	-0.03751	**0.11946**
$k_a^{PgL,Fn}$	0.0107	0	0	-0.03632	-0.00223	0.00608
$k_d^{PgL_B}$	0	0.0495	-0.00267	0.01168	0	0.00267
--	--	--	--	--	--	--
$k_{cat}^{PgG,Pn}$	-0.00803	0.06125	0.00343	-0.04339	0	-0.00142
$k_{cat}^{PgG_B,Pn}$	-0.01873	0.03948	0	-0.00485	-0.00223	0.01558
$k_{cat}^{Fn,Pn}$	**0.1338**	**-0.09023**	0.07206	**-0.1596**	0.04991	**-0.16347**
$k_{cat}^{PgG_B,TPA_B}$	**0.14182**	**-0.07348**	0.07206	**-0.17983**	0.04991	**-0.15766**
$k_{cat}^{PgL_B,TPA_B}$	-0.0107	-0.03168	0	0.03145	0	-0.00523
$k_{cat}^{PgG,TPA}$	0.0107	-0.03457	0	-0.01288	0	-0.00257
$k_{cat}^{PgL,TPA}$	0.0107	0.04834	0	-0.01614	0	0
--	--	--	--	--	--	--
$k_i^{TPA,PAI-1}$	-0.08831	-0.23535	-0.02287	-0.16472	-0.01367	-0.12392
k_i^{Pn,α_2M}	0	-0.03746	0	-0.02968	0	0.01577
k_i^{Pn,α_2AP}	-0.0107	0.05402	0	-0.03884	0	-0.00104
k_i^{PgL,α_2AP}	0	0.00318	0	-0.00972	0	0
$k_i^{Pn_B,\alpha_2AP}$	**-0.1338**	**0.15032**	-0.06519	**0.22183**	-0.03974	**0.19788**
$k_i^{PgL_B,\alpha_2AP}$	0	0	0	0	0	0
--	--	--	--	--	--	--
D_{PgG}	0.00803	-0.05576	0	-0.02268	0	0.01216
D_{PgL}	-0.00803	0.02581	0	-0.01269	0	-0.00143
D_{Pn}	0.00803	-0.04343	-0.00343	0.00625	0	-0.01035
D_{TPA}	**0.56195**	**0.40012**	**0.50324**	**0.39141**	**0.49496**	**0.43393**
D_{PAI1}	-0.07225	**0.13693**	-0.00343	**0.11592**	0.00223	0.06149

Table S6. The values of C^S and C^W obtained for a range of TPA concentrations in the presence of flow.

	TPA 10 nM		TPA 100 nM		TPA 1000 nM	
	C^S 5%	**C^W 5%**	**C^S 5%**	**C^W 5%**	**C^S 5%**	**C^W 5%**
Fn	0.01187	**-0.22471**	-0.0201	**-0.23465**	0	**-0.20418**
α_2M	0.04089	0.02171	-0.03115	-0.02048	-0.00957	0.0075
α_2AP	0.00739	**0.38183**	-0.01447	**0.24339**	-0.04169	**0.14625**
TPA	0.05988	**-0.29477**	0.0402	**-0.13984**	0.05878	-0.06995
PgG	-0.03825	**-0.38453**	0.04924	**-0.24741**	0.03896	**-0.1821**
PAI-1	-0.08626	**-0.08387**	-0.06029	**-0.12638**	-0.11482	**-0.14037**
--	--	--	--	--	--	--
$k_a^{Pn,Fn}$	0.07202	0.03188	-0.03477	-0.00909	0.01709	0.01791
$k_d^{Pn_B}$	0.01451	-0.00226	-0.06029	-0.01614	0.00478	-0.01539
$k_a^{TPA,Fn}$	-0.05988	**-0.30833**	-0.01105	**-0.27163**	0.00752	**-0.21209**
$k_d^{TPA_B}$	0.0335	0.03503	-0.0201	-0.00169	0	0.00711
$k_a^{PgG,Fn}$	0.08626	**-0.22516**	0	**-0.16269**	0.00478	**-0.10621**
$k_d^{PgG_B}$	-0.07914	**0.20299**	-0.0402	**0.15094**	-0.02666	**0.09622**
$k_a^{PgL,Fn}$	-0.0525	-0.04181	0	-0.00305	0.06835	0.05582
$k_d^{PgL_B}$	0	0.00407	-0.0201	-0.01545	-0.06835	-0.01336
--	--	--	--	--	--	--
$k_{cat}^{PgG,Pn}$	0.05276	0.02668	-0.0402	-0.0222	-0.00752	0.01336
$k_{cat}^{PgG_B,Pn}$	-0.07914	-0.03142	0.00543	-0.00303	0.0123	-0.00836
$k_{cat}^{Fn,Pn}$	0.01451	**-0.34068**	0.12059	**-0.16947**	0.05126	**-0.14542**
$k_{cat}^{PgG_B,TPA_B}$	0.02612	**-0.31446**	0.10049	**-0.18186**	0.05605	**-0.13747**
$k_{cat}^{PgL_B,TPA_B}$	0.03799	0.0052	0	0.00739	-0.06356	-0.03041
$k_{cat}^{PgG,TPA}$	-0.09101	-0.02848	0.0402	0.00268	0.08544	0.01959
$k_{cat}^{PgL,TPA}$	0.02638	0.01583	0.03457	0.01243	0.08544	0.00253
--	--	--	--	--	--	--
$k_i^{TPA,PAI-1}$	-0.09075	-0.0676	-0.03115	-0.02519	-0.06066	-0.02585
k_i^{Pn,α_2M}	0.07914	0.04452	0.01467	0.0044	-0.06083	0.00123
k_i^{Pn,α_2AP}	0.0525	0.03504	-0.01467	-0.01513	-0.02666	-0.01622
k_i^{PgL,α_2AP}	-0.06015	-0.03709	0.02914	0.01345	-0.06835	-0.01626
$k_i^{Pn_B,\alpha_2AP}$	-0.01926	**0.35331**	-0.01105	**0.18861**	0.05878	**0.13877**
$k_i^{PgL_B,\alpha_2AP}$	-0.00718	-0.0182	0.00566	0.00875	0	0.00332
--	--	--	--	--	--	--
D_{PgG}	0.05276	0.03051	-0.01467	0.00234	-0.05605	-0.01043
D_{PgL}	-0.03377	-0.02395	-0.10049	-0.05044	0	-0.01584
D_{Pn}	-0.02612	-0.01311	0.01447	0.01612	0.00478	0.01874
D_{TPA}	0.00712	**0.14356**	**0.12943**	**0.33581**	**0.25613**	**0.46492**
D_{PAI1}	-0.00712	-0.03187	0.03477	0.00774	0	-0.01171

The hydrostatic pressure difference was 100 Pa. The initial fibrin clot porosity was 0.99, and the permeability was 10^{-13} m^2.

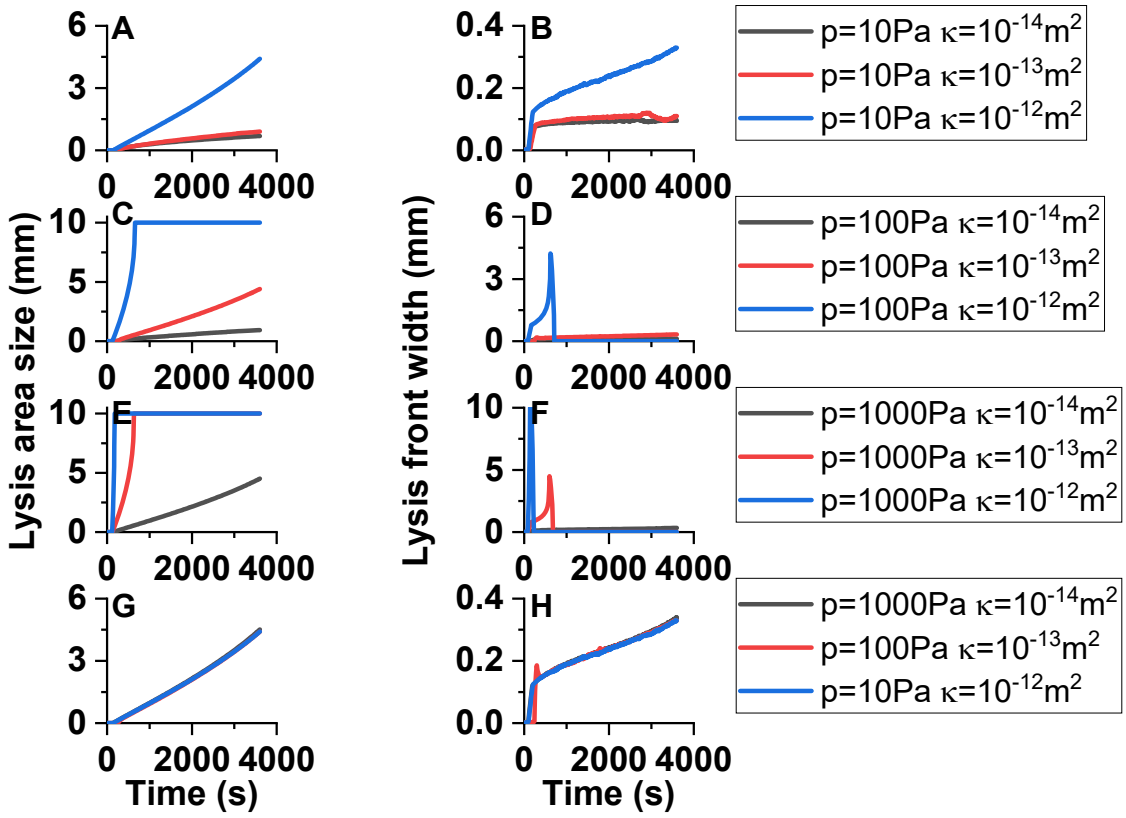

Fig. S6. Dependence of the spatial lysis process on the hydrostatic pressure difference and clot permeability. The initial TPA concentration was 30 nM. The initial clot porosity was 0.99. Panels A-B: hydrostatic pressure difference 10 Pa, (A) lysis area size, (B) lysis front width. Panels C-D: hydrostatic pressure difference 100 Pa, (C) lysis area size, (D) lysis front width. Panels E-F: hydrostatic pressure difference 1000 Pa, (E) lysis area size, (F) lysis front width. Black – clot permeability 10^{-14} m^2; red - clot permeability 10^{-13} m^2; blue - clot permeability 10^{-12} m^2. Panels G-H: Comparison of lysis area size (G) and lysis front width (H) for hydrostatic pressure 1000 Pa and clot permeability 10^{-14} m^2 (black), for hydrostatic pressure 100 Pa and clot permeability 10^{-13} m^2 (red), and for hydrostatic pressure 10 Pa and clot permeability 10^{-12} m^2 (blue). The increase in hydrostatic pressure generated an identical lysis response to that produced by the increase in clot permeability, as the curves in panels G and H are indistinguishable.

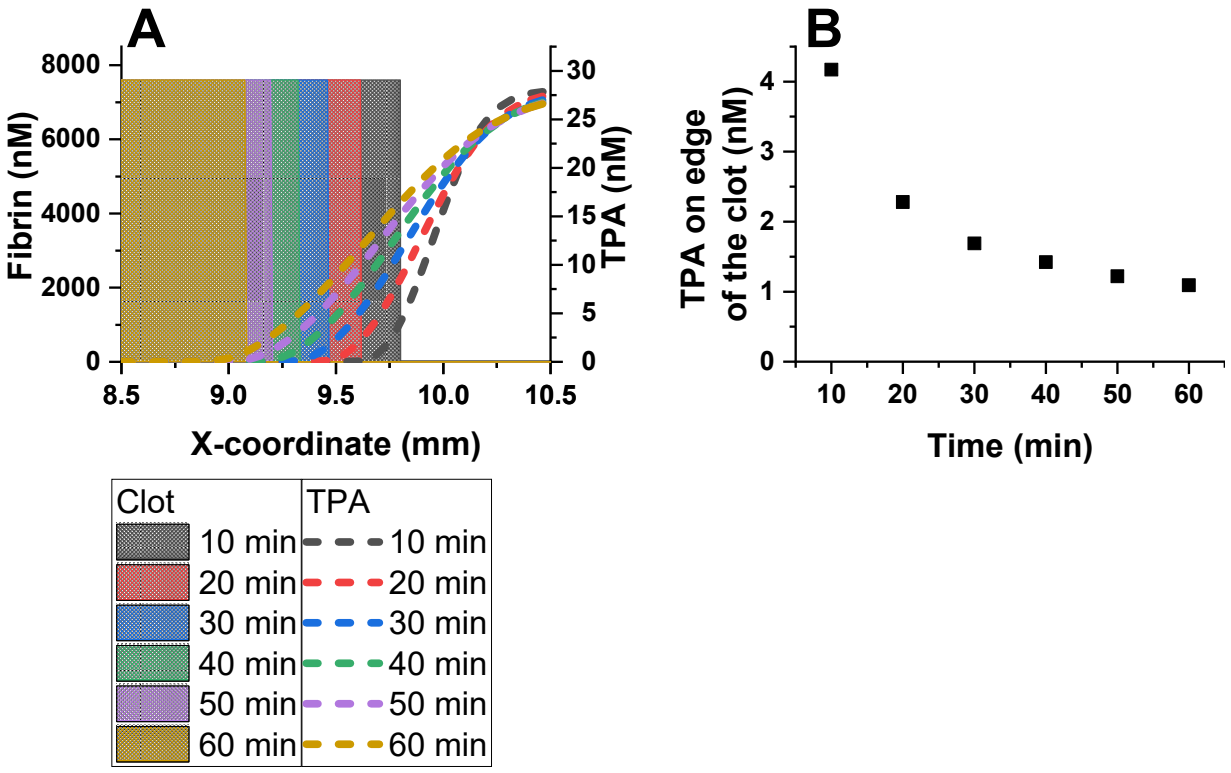

Fig. S7. Dynamics of fibrin clot lysis in the presence of flow. (A) TPA distribution (dashed lines) is shown for every 10 minutes of simulation. The filled area represents the current clot size (i.e., area where the fibrin concentration is above 50% of the initial concentration). (B) TPA concentration on the edge of the solid clot. Simulations were performed in the 1D model. The TPA concentration outside the clot was 30 nM. The hydrostatic pressure difference was 10 Pa, and the clot permeability was 10^{-13} m^2.

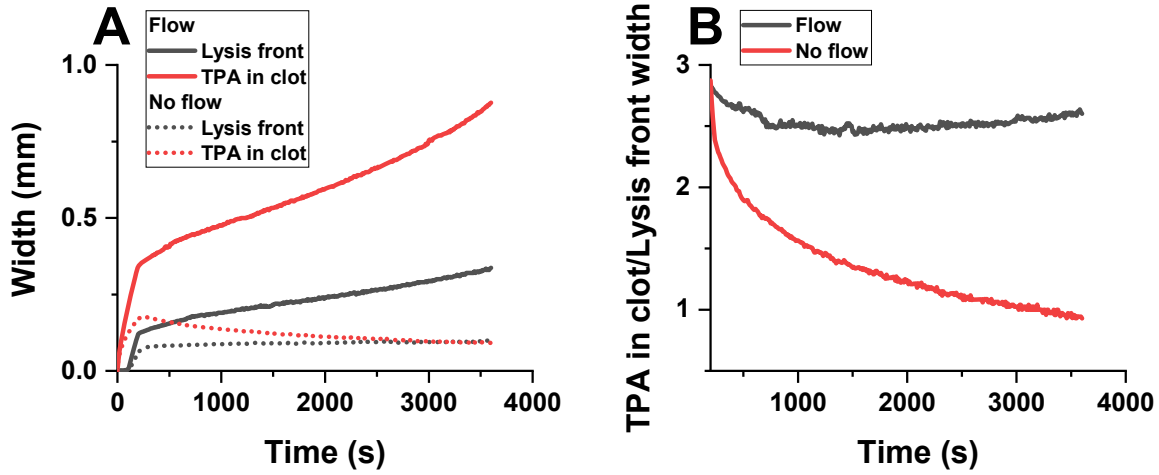

Fig. S8. Dynamics of TPA permeation in the clot. (A) Time course of lysis front width (black) and the zone of TPA penetration in the clot (red) in the presence of flow (solid lines) or in the absence of flow (dotted lines). (B) Ratio of the TPA penetration zone to lysis front width in the presence of flow (black) and in the absence of flow (red). Simulations were performed in the 1D model. The TPA concentration outside the clot was 30 nM. Under flow conditions, the hydrostatic pressure

difference was 100 Pa, and the clot permeability was 10^{-13} m^2. The zone of TPA penetration in the clot was determined as the size of the area, where 1) the fibrin concentration was higher than 25% of the initial (same as the condition for lysis front width), and 2) the TPA concentration was greater than the PAI-1 concentration.

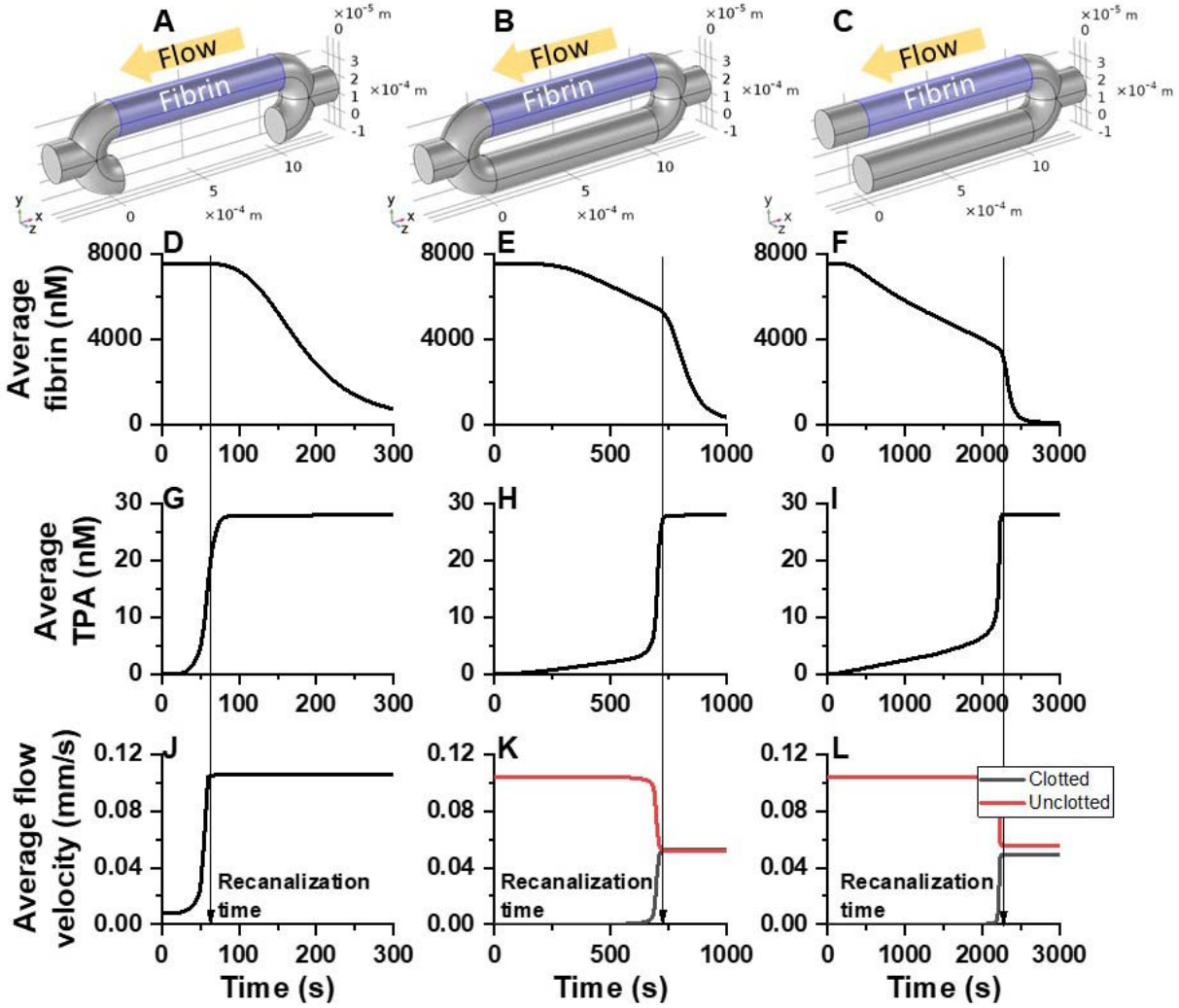

Fig. S9. Spatial lysis in the chamber with a single channel (A), with collateral channels and a single exit (B) or in a chamber with collateral channels and separate exits (C). Time course of the average fibrin concentration in the occluded vessel is shown in panels D, E and F; average free TPA concentration in the occluded vessel is shown in panels G, H and I; average flow velocity in the occluded and bypassing vessels is shown in panels J, K and L. Simulations were performed in the 3D model. The hydrostatic pressure difference was 100 Pa, the clot permeability was 10^{-13} m^2, and the initial clot porosity was 0.99. The chamber was constructed from tubes 200 μm in diameter, and the initial fibrin clot length was 1 mm.

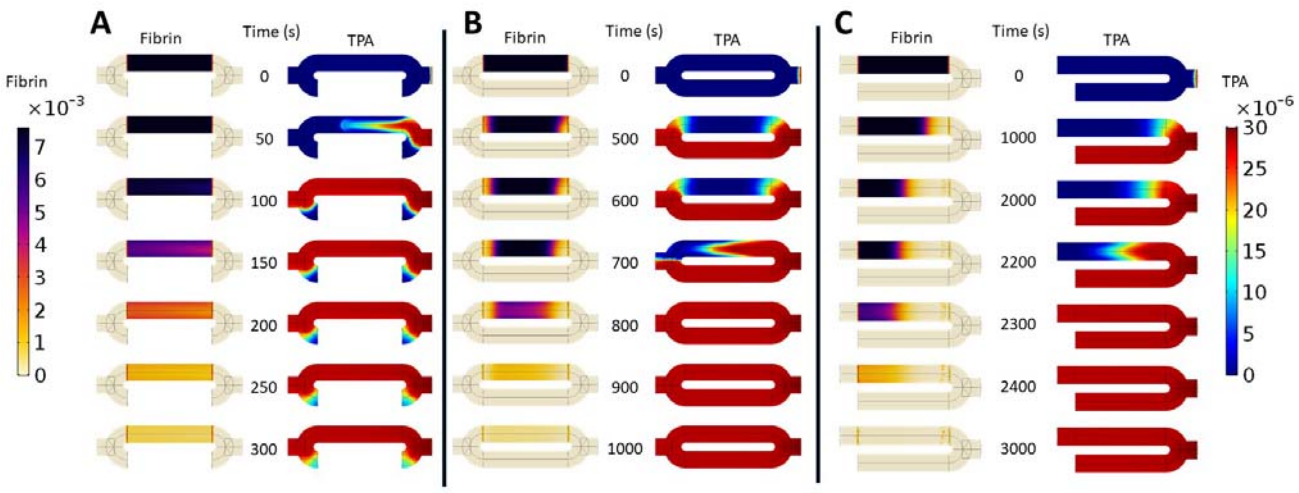

Fig. S10. Spatial distribution of fibrin and TPA in the chamber with a single channel (A), with collateral channels and a single exit (B) or with collateral channels and separate exits (C). Simulations were performed in the 3D model. The hydrostatic pressure difference was 100 Pa, the clot permeability was 10^{-13} m^2, and the initial clot porosity was 0.99.

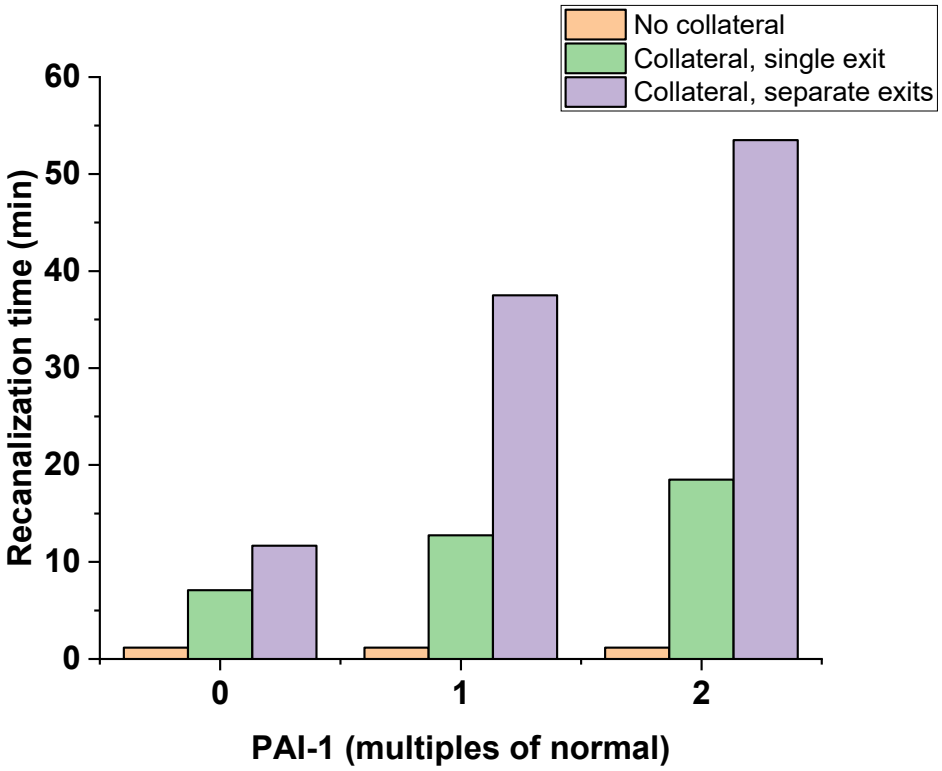

Fig. S11. Recanalization time drastically depends on PAI-1 concentration in the presence of collateral vessels, especially with separate exits. Simulations were performed in a 3D model. Hydrostatic pressure difference was 100 Pa, clot permeability was $10^{-13}m^2$, the initial clot porosity was 0.99.

1. Butenas, S., and K.G. Mann. 2002. Blood coagulation. Biochemistry. (Mosc). 67: 3–12.

2. Collen, D. 1999. The plasminogen (fibrinolytic) system. Thromb. Haemost. 82: 259–70.
3. Yoshino, S., K. Fujimoto, T. Takada, S. Kawamura, J. Ogawa, Y. Kamata, Y. Kodera, and M. Shichiri. 2019. Molecular form and concentration of serum α2-macroglobulin in diabetes. Sci. Rep. 9: 12927.
4. Tanswell, P., U. Tebbe, K.L. Neuhaus, L. Gläsle-Schwarz, J. Wojcik, and E. Seifried. 1992. Pharmacokinetics and fibrin specificity of alteplase during accelerated infusions in acute myocardial infarction. J. Am. Coll. Cardiol. 19: 1071–5.
5. Tebbe, U., P. Tanswell, E. Seifried, W. Feuerer, K.H. Scholz, and K.S. Herrmann. 1989. Single-bolus injection of recombinant tissue-type plasminogen activator in acute myocardial infarction. Am. J. Cardiol. 64: 448–53.
6. Tanswell, P., E. Seifried, P.C. Su, W. Feuerer, and D.C. Rijken. 1989. Pharmacokinetics and systemic effects of tissue-type plasminogen activator in normal subjects. Clin. Pharmacol. Ther. 46: 155–62.
7. Brott, T.G., E.C. Haley, D.E. Levy, W. Barsan, J. Broderick, G.L. Sheppard, J. Spilker, G.L. Kongable, S. Massey, and R. Reed. 1992. Urgent therapy for stroke. Part I. Pilot study of tissue plasminogen activator administered within 90 minutes. Stroke. 23: 632–40.
8. Weisel, J.W. 2005. Fibrinogen and fibrin. Adv. Protein Chem. 70: 247–99.
9. Collet, J.P., D. Park, C. Lesty, J. Soria, C. Soria, G. Montalescot, and J.W. Weisel. 2000. Influence of fibrin network conformation and fibrin fiber diameter on fibrinolysis speed: dynamic and structural approaches by confocal microscopy. Arterioscler. Thromb. Vasc. Biol. 20: 1354–61.
10. Wiman, B., H.R. Lijnen, and D. Collen. 1979. On the specific interaction between the lysine-binding sites in plasmin and complementary sites in α2-antiplasmin and in fibrinogen. Biochim. Biophys. Acta - Protein Struct. 579: 142–154.
11. Chmielewska, J., M. Rånby, and B. Wiman. 1988. Kinetics of the inhibition of plasminogen activators by the plasminogen-activator inhibitor. Evidence for “second-site” interactions. Biochem. J. 251: 327–32.
12. Higgins, D.L., and G.A. Vehar. 1987. Interaction of one-chain and two-chain tissue plasminogen activator with intact and plasmin-degraded fibrin. Biochemistry. 26: 7786–91.
13. Suenson, E., and S. Thorsen. 1988. The course and prerequisites of Lys-plasminogen formation during fibrinolysis. Biochemistry. 27: 2435–43.
14. Lucas, M.A., L.J. Fretto, and P.A. McKee. 1983. The binding of human plasminogen to fibrin and fibrinogen. J. Biol. Chem. 258: 4249–56.
15. Rånby, M. 1982. Studies on the kinetics of plasminogen activation by tissue plasminogen activator. Biochim. Biophys. Acta. 704: 461–9.
16. Wiman, B., L. Boman, and D. Collen. 1978. On the kinetics of the reaction between human antiplasmin and a low-molecular-weight form of plasmin. Eur. J. Biochem. 87: 143–6.
17. Suenson, E., and S. Thorsen. 1981. Secondary-site binding of Glu-plasmin, Lys-plasmin and miniplasmin to fibrin. Biochem. J. 197: 619–28.
18. Kolev, K., I. Léránt, K. Tenekejiev, and R. Machovich. 1994. Regulation of fibrinolytic activity of neutrophil leukocyte elastase, plasmin, and miniplasmin by plasma protease inhibitors. J. Biol. Chem. 269: 17030–4.
19. Wu, J.H., and S.L. Diamond. 1995. A fluorescence quench and dequench assay of fibrinogen polymerization, fibrinogenolysis, or fibrinolysis. Anal. Biochem. 224: 83–91.
20. Zhalyalov, A.S., M.A. Panteleev, M.A. Gracheva, F.I. Ataullakhanov, and A.M. Shibeko. 2017. Co-ordinated spatial propagation of blood plasma clotting and fibrinolytic fronts. PLoS One. 12: e0180668.
21. Marshall, A.G. 1978. Biophysical chemistry: principles, techniques, and applications. Wiley New York.

22. Panteleev, M.A., A.N. Balandina, E.N. Lipets, M. V Ovanesov, and F.I. Ataullakhanov. 2010. Task-oriented modular decomposition of biological networks: trigger mechanism in blood coagulation. Biophys. J. 98: 1751–61.